DEPARTMENT OF PHYSICS
UNIVERSITY OF JYVÄSKYLÄ
RESEARCH REPORT No. 9/2012

A MONTE CARLO SIMULATION FOR THE ELASTIC ENERGY LOSS OF HIGH-ENERGY PARTONS IN A STRONGLY INTERACTING MEDIUM

BY
JUSSI AUVINEN

Academic Dissertation
for the Degree of
Doctor of Philosophy

To be presented, by permission of the
Faculty of Mathematics and Natural Sciences
of the University of Jyväskylä,
for public examination in Auditorium FYS-1 of the
University of Jyväskylä on August 31, 2012
at 12 o'clock noon

Jyväskylä, Finland
June 2012

Preface

The work presented in this thesis has been done at the Department of Physics in the University of Jyväskylä over the years 2007-2011.

First and foremost, I would like to thank my two supervisors, Prof. Kari J. Eskola and Dr. Thorsten Renk, who, with great patience and perseverance, have educated me about the fascinating physics of ultrarelativistic heavy ion collisions over all these years. I would also like to thank Dr. Hannu Holopainen for the smooth collaboration and providing the hydrodynamical backgrounds for several of the studies presented in this thesis. Dr. Harri Niemi deserves also credit, having done the hydrodynamical simulations utilized in the first Paper. Special thanks to Prof. Paul Hoyer and Prof. Kari Rummukainen for reviewing the original manuscript of this thesis, and to Prof. Steffen A. Bass for agreeing to act as my opponent.

All my other friends and colleagues, past and present, along with the other personnel in the Department of Physics, warrant also appreciation for creating a very enjoyable working environment. And, as always, I am grateful to my parents and other relatives for all their support during this long journey.

The financial support from the Jenny and Antti Wihuri Foundation and the Academy of Finland, the projects 115262 and 133005, is very gratefully acknowledged. In addition, CSC - IT Center for Science in Espoo, Finland is acknowledged for the allocation of computational resources.

List of publications

This thesis is based on the work contained within the following publications:

I **A Monte-Carlo model for elastic energy loss in a hydrodynamical background**
J. Auvinen, K. J. Eskola and T. Renk,
Phys. Rev. C **82**, 024906 (2010) [arXiv:0912.2265 [hep-ph]].

II **Elastic energy loss with respect to the reaction plane in a Monte-Carlo model**
J. Auvinen, K. J. Eskola, H. Holopainen and T. Renk,
Phys. Rev. C **82**, 051901 (2010) [arXiv:1008.4657 [hep-ph]].

III **Monte Carlo Simulation for Elastic Energy Loss of Hard Partons in a Hydrodynamical Background**
J. Auvinen, K. J. Eskola, H. Holopainen and T. Renk,
J. Phys. G **38**, 124160 (2011) [arXiv:1106.4167 [hep-ph]].

IV **Energy loss in a fluctuating hydrodynamical background**
T. Renk, H. Holopainen, J. Auvinen and K. J. Eskola,
Phys. Rev. C **85**, 044915 (2012) [arXiv:1105.2647 [hep-ph]].

V **The form of the elastic energy loss probability distribution in a static medium**
J. Auvinen and T. Renk,
Phys. Rev. C **85**, 037901 (2012) [arXiv:1112.1779 [hep-ph]].

The author has developed from scratch the elastic energy loss Monte Carlo simulation code which has been used in all the papers listed above. The author has written the draft versions of the papers [I-III] and [V] and participated in planning and writing of paper [IV].

Contents

Chapter 1

Introduction

Particle accelerator experiments have been the main method of investigation for particle physics in the 20th and 21st century. The precursor of these was the famous Rutherford experiment in 1909 where Hans Geiger and Ernest Marsden, under the direction of Ernest Rutherford, shot a beam of α particles (He^{2+}) into a gold foil [1]. The results of this experiment led Rutherford to formulate his atom model in 1911, where negatively charged electrons orbit the dense, positively charged nucleus [2]. He named the nucleus of a hydrogen atom as *proton* in 1920 [3]. The discovery of *neutron* by James Chadwick in 1932 [4] completed the elementary picture of the atom.

Further examination of the protons and neutrons requires probes with wavelengths small enough to resolve the finer details. As the de Broglie wavelength of a particle is inversely proportional to its momentum, $\lambda = \frac{h}{p}$ (h being the Planck constant) [5], higher resolutions require higher energies. In the latter half of the 20th century, the available energies in the particle accelerators had grown large enough to probe the structure of protons and neutrons. The electron-proton deep inelastic scattering measurements done at Stanford Linear Accelerator Center (SLAC) in 1968 [6, 7] confirmed that the proton, in turn, consists of point-like spin-1/2 particles. This was also consistent with the model by Gell-Mann [8] and Zweig [9], where the proton was assumed to be composed of three spin-1/2 particles with fractional charges. Gell-Mann had named these particles *quarks*[1] [8].

The theory of quarks and strong interaction, mediated by *gluons*, is called Quantum Chromodynamics (QCD)[2]. It secured its position as the prevalent theory for elementary particles (in addition to QED, Quantum Electrodynamics and its unification with the weak interactions) in 1974 when a new particle J/ψ was simultaneously discovered in electron-positron collisions at SLAC [11]

[1]Nowadays, with the more refined understanding of the theory of strong interaction, it is understood that all the hadrons (i.e. particles consisting of quarks and/or antiquarks) have 2 or 3 *valence* quarks, but in addition of these, there is also an immeasurable amount of virtual quarks and antiquarks (known as sea quarks) and gluons.

[2]For an early review, where the name "Quantum Chromodynamics" was first used, see Ref. [10].

and in Brookhaven National Laboratory (BNL), where Alternating Gradient Synchrotron (AGS) was used for fixed target p+Be experiment [12]. According to the quark model, J/ψ is a bound state of a charm quark and its antiquark. Most importantly, the model predicted that several other "charmed" particles should be found. Charmed baryons were discovered in BNL the following year [13] and charmed mesons in SLAC a year after that [14, 15].

Already in 1975 it was realized that, for very high temperatures or (baryon) matter densities, QCD implies the existence of a state of matter consisting of quarks which are not confined in hadrons [16, 17]. The lattice QCD calculations a few years later also suggested a phase transition [18, 19]. Edward Shuryak named this QCD phase of matter "Quark-Gluon Plasma" (QGP) in his 1980 review of QCD and the theory of superdense matter [20]. The properties of such a deconfined phase are of interest not only to particle physics, but also cosmology (the physics of the early Universe) and astrophysics (the properties of the matter inside neutron stars). However, the accelerators of that time could not produce collisions with the supposedly required energy densities of the order 1 GeV/fm^3 [21]. To achieve such densities, a large number of high-energy particles must be produced in a small spacetime region; thus, heavy ion collisions are needed.

The Super Proton Synchrotron (SPS) in CERN started looking for the QGP signatures with O+Pb collisions in 1986. The center-of-mass energy per colliding nucleon pair ($\sqrt{s_{NN}}$) in these experiments was 19.4 GeV [22]. Nothing decisive about the existence of QGP was found in these or the later experiments with sulphur, so in 1994 a heavier Pb beam was introduced for the new experiments with collision energies $\sqrt{s_{NN}} \approx 17$ GeV. In the beginning of the year 2000, the SPS experiments had collected enough suggestive evidence (such as the multiplicity and momentum distributions of hadrons, excess of dileptons, enhancement of hadrons with strangeness, suppression of charmonium states) [23] for CERN to announce the discovery of the new state of matter [24].

The Relativistic Heavy Ion Collider (RHIC) at the Brookhaven National Laboratory (BNL) started its operation in the year 2000. During the following years, RHIC reached its top center-of-mass energy $\sqrt{s_{NN}} = 200$ GeV and the four experiments BRAHMS [25], PHENIX [26], PHOBOS [27] and STAR [28] confirmed the existence of the quark-gluon plasma [29–32] (compilation of the papers can be found at [33]). There are several hadronic observables supporting the formation of the QGP in the Au+Au collisions at RHIC:

1) *Particle multiplicity:* Lattice QCD studies suggest that the required energy density for the formation of quark-gluon plasma is of the order of 1 GeV/fm^3 [34]. Unfortunately, the energy density cannot be directly measured, but it can be estimated from the amount of particles produced in a collision combined with the average energy per particle. The charged particle multiplicities, and in particular the transverse energy of these particles, observed at RHIC [35–38] allow estimates for the lower limit of the initial energy density which vary from 3 GeV/fm^3 [31] to 15 GeV/fm^3 [30] – this would be quite enough for the formation

of the QGP.

2) *Elliptic flow:* If a heavy ion collision is non-central, the transverse overlap region of the two colliding nuclei has the shape of an ellipse instead of a circle ("spatial anisotropy"). If there are sufficient scatterings in the early stage to establish local thermal equilibrium, then the pressure gradient will be largest in the shortest direction of the ellipse, producing eventually higher particle transverse momenta in that direction ("momentum anisotropy").

The azimuthal momentum distribution of the produced particles is usually parametrized as a Fourier series with terms of the form $v_n(p_T)\cos(n\phi)$, where ϕ is the angle relative to the reaction plane. The $n = 2$ term measures the elliptic flow and thus the coefficient v_2 is often used synonymously with it. Already in the measurements with collision energy $\sqrt{s_{NN}} = 130$ GeV, the measured v_2 was found to approximately scale with the initial eccentricity of the overlap region in the transverse momentum range $0.4 < p_T < 0.6$ GeV/c [39]. This indicates collective behavior early in the collision event, supporting the argument presented above. The later experiments with the top energy $\sqrt{s_{NN}} = 200$ GeV produced even clearer signals for the elliptic flow [30, 40, 41].

3) *Suppression of single high-energy hadrons:* Long before RHIC, the theorists predicted that one signal for the formation of quark-gluon plasma in a heavy ion collision should be the reduced yield of high-energy hadrons (see Chapter 2). To measure this, the *nuclear modification factor* for a hadron h, R^h_{AA}, is defined as

$$R_{AA}(p_T, y) = \frac{d^2N^{AA\to h+X}/dp_T dy}{\langle N^{AA}_{\rm bin}\rangle d^2N^{pp\to h+X}/dp_T dy}, \tag{1.1}$$

where $d^2N^{AA\to h+X}/dp_T dy$ is the measured inclusive particle spectrum for hadron h in the heavy ion collisions, $d^2N^{pp\to h+X}/dp_T dy$ is the measured spectrum in the p+p collisions and $\langle N^{AA}_{\rm bin}\rangle$ is the expected (average) number of binary nucleon-nucleon collisions in a heavy ion collision in a given centrality class (this is discussed in more detail in Chapter 3).

In the absence of any new physics – such as the formation of a medium – one would expect the nuclear modification to be close to unity. This was found to be approximately true for the most peripheral collisions in RHIC experiments. However, in the most central collisions, the R_{AA} was found to be ~ 0.2 for $p_T > 5$ GeV/c for both neutral pions and charged hadrons [42–44]. Such suppression is absent in d+Au collisions with the same energy [45, 46], indicating that the suppression in central Au+Au collisions is not due to the initial-state effects such as parton saturation in a color glass condensate [47] or nuclear effects in parton structure functions. Rather, it stems from the interactions of the high-energy particle with the medium formed in these heavy ion collisions. This is also supported by the fact that the nuclear modification for photons (which do not participate in strong interactions) is close to unity even in Au+Au collisions [48].

4) *Jets and dihadron correlations:* The nuclear modification factor is a single-particle observable. However, the high-energy partons originating from the initial nucleon-nucleon collisions each fragment into a jet of hadrons and thus, to

get a more complete picture of the energy loss of these hard partons, it would be useful to identify these jets and analyze their structure.

In practice, jet reconstruction in the heavy ion collisions is a highly nontrivial task due to the presence of large background of soft particles. One way to examine jets is to study the two-hadron azimuthal angle correlations. Here one particle acts as a "trigger", detected in a certain p_T range, while the other, "associated", particle will be picked from a lower p_T region. After the two hadrons have been chosen, their relative azimuthal angle $\Delta\phi$ is defined. When the yield of associated particles per trigger particle is plotted with respect to $\Delta\phi$, a peak is seen around $\Delta\phi = 0$ and another (broader) peak around $\Delta\phi = \pi$. These are the near side and away side jets, respectively.

The modification factor for dihadron correlations is $I_{AA}(p_T^{\mathrm{trigger}}, p_T^{\mathrm{assoc}}, \Delta\phi)$, which is the ratio of per-trigger yields of associated particles in A+A and p+p collisions for given momenta of trigger and associated particles and the angle $\Delta\phi$ between them.

The measurements at RHIC [49, 50] for the trigger particle with transverse momentum $p_T^{\mathrm{trigger}} > 4$ GeV/c show that in the most central collisions, the near-side I_{AA} is roughly one, while the away-side I_{AA} is $\approx 0.2 - 0.4$ for the associated particle $p_T^{\mathrm{assoc}} > 2$ GeV/c. The away-side suppression decreases towards more peripheral collisions and thus behavior of the away-side I_{AA} is very similar to the single-hadron R_{AA}. Although interpreting the dihadron modification requires more care than the nuclear modification factor [51], it is nevertheless safe to say that the results indicate some new final state physics emerging in the nucleus-nucleus collisions compared to proton-proton.

Altogether, the evidence for high energy densities, pressure formation (with the quark number scaling of the resultant flow) and the suppression of high-energy hadrons makes a convincing case for the formation of strongly interacting partonic medium in the heavy ion collisions at RHIC. Yet, determining the detailed properties of this QCD medium requires even higher energies.

The current state-of-the-art collider is the Large Hadron Collider (LHC) at CERN. It started its operation in November 2009 with p+p collisions at $\sqrt{s} = 900$ GeV, reaching its current maximum energy of $\sqrt{s} = 7$ TeV in March 2010. The first Pb+Pb heavy ion run was in November 2010, with the energy of $\sqrt{s_{NN}} = 2.76$ TeV. The LHC has six experiments running: ALICE [52], ATLAS [53], CMS [54], LHCb [55], TOTEM [56] and LHCf [57], with seventh, MoEDAL [58], in preparation. Of these, ALICE is dedicated to the physics of heavy ion collisions and both CMS and ATLAS run an active heavy ion program.

Due to the higher collision energy, the particle multiplicities in the LHC are over two times higher than at RHIC [59–61], corresponding to higher energy densities and hotter, longer existing quark-gluon plasma. The elliptic flow coefficient $v_2(p_T)$ is found to be only slightly larger than at RHIC [62–64]; for p_T-integrated flow ALICE reports a 30% increase [62]. In addition, also higher order coefficients v_3, v_4 and v_5 have been measured [65, 66], even v_6 [67]. The results agree remarkably well with the hydrodynamical predictions [68].

The nuclear modification factor R_{AA} for charged hadrons, measured by ALICE [69, 70] and CMS [71], is below the RHIC result; approximately 0.15 at its lowest point around $p_T = 6 - 7$ GeV/c in most central collisions. As a new feature, R_{AA} rises steeply after the minimum point until reaching a constant value between 0.4-0.5 for $p_T > 30$ GeV/c. ATLAS finds similar trend for their central-to-peripheral ratio R_{CP} [72].

The dihadron measurements by ALICE [73], with trigger $8 < p_T < 15$ GeV/c, show an enhancement on the near-side peak: $I_{AA} \approx 1.2$ in central collisions. This enhancement was expected [74], and it is due to a kinematic bias towards higher parton energy. The away-side peak is still suppressed, although only by a factor of two. In peripheral collisions $I_{AA} \approx 1$ for both near and away-side.

Improvements in detector technology and the emergence of jets with higher energies relative to the soft background in the LHC energies allows for more reliable jet reconstruction efforts. In order to quantify the softening and broadening of the jets due to the medium, ATLAS and CMS have measured the dijet asymmetry, which reflects the imbalance between the transverse energies E_{T1}, E_{T2} of the two jets: $A_J = \frac{E_{T1}-E_{T2}}{E_{T1}+E_{T2}}$ [75, 76]. In both experiments, the fraction of unbalanced (larger A_J) dijets is found to increase towards more central collisions, deviating considerably from the corresponding behavior in p+p collisions. Additionally, studies of the average missing transverse momentum by CMS [76] show that a large part of the balancing momentum is carried by low-momentum particles spreading to large angles with respect to the jet axis. All of this supports the concept of hard-parton energy loss in a strongly interacting medium.

The progress of science is founded on the interplay of theory and experiments. The Rutherford experiment necessitated a new theory of the atom structure. Halfway into the 20th century, unexpected new particles were discovered, which led to the development of the Quantum Chromodynamics. The QCD in turn posed an experimental challenge; the formation of the quark-gluon plasma.

The experiments during the past decade have successfully confirmed the theoretical expectations of the QGP forming in ultrarelativistic heavy ion collisions. This strongly interacting medium has an observed effect on the spectrum of produced hadrons – along with the electromagnetic observables such as photons – and now the task faced by the theorists is to formulate a QCD-based description, which correctly describes all the observations and enables the determination of the detailed properties of the quark-gluon plasma.

In this thesis, the energy loss of hard partons in a strongly interacting medium is studied with a Monte Carlo model specifically built for this purpose. The thesis consists of four original research papers [I, II, IV, V], a conference proceeding with a previously unpublished result [III] and an introductory part presented on the following pages. Chapter 2 is a brief review of the models for the high-energy hadron suppression in heavy ion collisions. Chapter 3 describes the basic concepts associated with the Monte Carlo energy loss model studied in this thesis. Chapter 4 presents the results of the Monte Carlo simulation, while the summary and outlook are provided in Chapter 5.

Chapter 2

Energy loss models

Modeling the suppression of high-P_T hadrons[1] in ultrarelativistic heavy ion collisions is a complicated task, which requires the modeling of the various stages of these collisions, as well as identifying the dominant energy loss mechanism.

In the initial state of every energy loss model, there are high-energy ("hard") partons which have been formed in the primary collision of two nucleons. In the final state, these partons must have fragmented into hadrons. During some phase of this evolution, there must be interactions with the medium, which cause the suppression of the hadron P_T-distribution.

Most models assume that the hard partons in the beginning are on-shell and the interactions with the medium, leading to energy loss, happen during this state of evolution. Usually only the highest-energy ("leading") parton is followed and only in the very end does this parton fragment into hadrons. One exception is the Higher Twist model [77–85], an analytical realization of the in-medium shower evolution, where the medium modification is implemented into the evolution of fragmentation functions.

There are also several Monte Carlo models – PYQUEN [86, 87], Q-PYTHIA [88], JEWEL [89,90], YAJEM [91–94] – which begin with the highly virtual hard partons, which reduce their virtuality by gluon radiation. This leads to a parton shower, which interacts with the medium and eventually transforms to a jet of hadrons when the virtuality reaches low enough scale.

Various assumptions can be also made about the nature of the medium. Depending on the model, the medium can be represented either as an ideal gas of massless partons or a collection of massive static scattering centers. The typical first approximation is to assume that there is no flow and the temperature remains constant, although most modern models do strive to include at least the 1-dimensional Bjorken evolution. Most advanced approaches can utilize even hydrodynamics with (3+1)-dimensional evolution equations.

The most essential part of any energy loss model is, naturally, the description of the interactions between the hard parton and the medium. There are two

[1]Starting from this Chapter, P_T is used to denote the hadron transverse momentum, while p_T is reserved for the parton transverse momentum.

main mechanisms: The elastic collisions between the hard parton and medium constituents, and the gluon radiation induced by the medium. The latter is complicated by the non-negligible formation time and the ensuing coherence effects; however, this also makes the radiative energy loss more sensitive to the geometry of the background medium.

In the following, a short historical review is provided, in order to illustrate how the energy loss modeling has evolved from simple estimates towards more elaborate schemes over the past few decades. The role of the energy loss model developed in this thesis will be discussed in Section 2.6.8.

2.1 First estimates

First estimates of the hard parton energy loss were made already in 1982 by Bjorken [95]. He studied the propagation of a massless high-energy parton through an ideal uniform quark-gluon gas in a thermal equilibrium. For the $2 \to 2$ scattering amplitudes, the small momentum transfers were assumed to be dominant[2]. For the upper and lower limits of the energy transfer, Bjorken used $|t_{\max}| = s/2$ and $|t_{\min}| = M^2$, where $\sqrt{s}$ is the center-of-mass energy of the collision and $M \approx 0.5 - 1$ GeV corresponds to the thermal (Debye) mass. The average energy loss per unit length $\frac{dE}{dx}$ was actually rather weak, ~ 0.1 GeV/fm for a 20-GeV particle with the coupling strength $\alpha_s = \frac{g_s^2}{4\pi} = 0.2$ in a medium with temperature $T = 0.25$ GeV. This is notably less than the estimated dynamic string tension $\approx 1-2$ GeV associated with the parton fragmenting into a jet of hadrons [96], suggesting that the signal for QGP formation might in fact be jet *un*quenching [97]. On the other hand, Svetitsky [98] studied the drag and diffusion of charm quarks in a uniform quark-gluon plasma and found a strong damping of heavy quarks (they would, as a matter of fact, thermalize in this scenario).

At the beginning of the '90s, Thoma and Gyulassy (TG) [99] studied the quark energy loss caused by the Lorentz force of the chromoelectric field induced by the high-energy quark in a high-temperature quark-gluon plasma. This calculation corresponds to elastic scattering via an exchange of a hard thermal loop (HTL) gluon, thus properly accounting for the plasma screening (characterized by the Debye mass $\mu_D \sim g_s T$ [100]) in the lower limit of the momentum transfer exchange. In the upper limit, the maximum possible momentum of the transferred gluon was taken to be equal to the hard quark momentum (in the case of massless quarks; for massive quarks, the limit has temperature dependence). The energy loss in this scenario was once again found to be weak: $\frac{dE}{dx} = 0.2$ GeV/fm – and even less for massive quarks – with the same parameters as in the Bjorken's estimate above.

Braaten and Thoma (BT) [101,102] aimed to construct a model with natural

[2]This is the so-called "Mandelstam t-channel" approximation; the Mandelstam variables are defined in the scattering rate section of Chapter 3.

limits for both small and high energy transfers. They introduced an intermediate energy scale q^*. Above this scale, the calculations were made with tree-level $2 \to 2$ Feynman diagrams ignoring screening (hard contribution), while below the scale the screening was taken into account using the HTL resummed perturbation expansion (soft contribution). Adding together the hard and soft contributions removed the dependence on the intermediate scale. The results for heavy quark energy loss were of the same order of magnitude as the results by Bjorken (adapted version for heavy quarks) and TG.

Gyulassy, Plümer, Thoma and Wang proceeded to estimate the radiative energy loss in a Bjorken-type calculation using Gunion-Bertsch radiation spectrum [103] and concluded that it would dominate over elastic in quark-gluon plasma [104, 105]. Thus the focus of energy loss modeling moved to the radiative side.

2.2 Radiative energy loss for static scatterers

Gyulassy and Wang [106], with Plümer [107], began investigating the problem of the Landau-Pomeranchuk-Migdal (LPM) effect [108] for medium-induced soft radiation in QCD. The characteristic property of forward (i.e. small angle) radiation is the non-zero formation time $\tau_f \sim \frac{2\omega}{k_T^2}$, where ω is the energy of the radiated gluon and k_T ($\ll \omega$) is the transverse momentum of the gluon with respect to the parent parton direction. The formation (or "separation") time can be interpreted as the time required to separate the wavepackets of the radiated gluon and the hard parton from each other. When the parton's mean free path λ in the medium is less than the formation time of the radiative process, destructive interference occurs between successive radiation amplitudes, suppressing the radiation.

In order to simplify the calculations, the system was assumed to consist of static scattering centers in a constant temperature T, separated by distances much larger than the Debye screening length μ_D^{-1}. When the parton with high energy E interacts with a scattering center, it radiates a gluon with energy ω which, in the soft radiation limit, is much smaller than E. The change on the trajectory of the hard parton can then be considered negligible (this is known as "eikonal approximation").

Based on the calculations of this model in the limit $k_T < \mu_D$, about 75% of the total energy loss would come from the radiative processes for a 30-GeV quark in a static medium of temperature $T = 300$ MeV with strong coupling $\alpha_s = 0.3$.

2.2.1 BDMPS-Z

Baier, Dokshitzer, Peigne and Schiff (BDPS) further elaborated on the Gyulassy-Wang model by taking into account the n rescatterings of the radiated gluon in

the (infinite) static medium [109], which modify k_T (by a total of $\sim O(n\mu_D)$) and therefore the formation time. This was found to increase the radiative energy loss per unit length compared to the previous results. Later BDPS refined the model further in collaboration with Mueller [110] and the model became known as BDMPS.

Studies of the medium with finite size L [111, 112] led to a surprising result: The square-pathlength dependence of the radiative energy loss, $\Delta E \propto L^2$. How the coherent nature of radiative energy loss leads to L^2 dependence can be seen by estimating the maximum energy $\omega_{\max}$ the hard parton can lose by radiating a gluon within a pathlength L [111]. The gluon energy ω is limited by the formation time $\tau_f = \frac{2\omega}{k_T^2} \leq L$. The maximum transverse momentum the gluon can achieve within L is $k_{T\max}^2 = \frac{L}{\lambda_g}\mu^2$, where λ_g is the mean free path of the gluon and μ is the typical momentum transfer in a scattering. Thus the maximum energy lost by the hard parton is $\Delta E = \omega_{\max} = \frac{1}{2}Lk_{T\max}^2 = \frac{1}{2}\frac{\mu^2}{\lambda_g}L^2$.

The L^2-behavior of the radiative energy loss is a critical difference compared to elastic energy loss, for which $\Delta E \propto L$. Thus the result suggests that the pathlength-dependence measurements of the hadron suppression have potential to reveal whether the energy loss is mainly coherent (like the radiative processes described above) or incoherent (as in elastic collisions).

The predictive power of the BDMPS model in the nucleus-nucleus collisions is however weakened by the assumption of the static medium. To remedy the situation, the attempt was made by Baier, Dokshitzer, Mueller and Schiff (BDMS) [113] to implement the simple Bjorken hydrodynamical model [114] into the formalism: At initial time τ_0, where the proper time is defined as $\tau = \sqrt{t^2 - z^2}$, the medium has temperature T_0. The high-energy quark travels in the direction transverse to the beam axis while the medium expands into longitudinal z-direction. The system cools down as a function of τ according to the scaling law $\tau^\alpha T^3 = \tau_0^\alpha T_0^3$, where the parameter α can vary between 0 (static, constant-temperature medium) and 1 (ideal relativistic plasma). For the transverse plane $z = 0$, this corresponds to $t^\alpha T^3 = t_0^\alpha T_0^3$, providing a time-dependence to the temperature-dependent BDMPS parameters μ_D and λ. The energy loss was found to be up to 6 times larger compared to the static case, when the comparison was made in the same *final* temperature, meaning that the parton in evolving medium had experienced larger densities while traveling the distance L.

In the meanwhile, Zakharov had developed his own method for calculating the medium-induced radiative energy loss; the "light cone path integral approach" (LCPI) [115–117]. In this approach, the calculation of the radiation rate is reformulated into solving a certain two-dimensional Schrödinger equation with an imaginary potential, which is proportional to the cross section of a color neutral quark-antiquark-gluon state interacting with a static scattering center in the medium. Amazingly, this method was shown to be equivalent with the BDMPS by Baier *et al.* [118] and so the formalism is nowadays known as

BDMPS-Z.

2.2.2 GLV

In the BDMPS formalism, it was assumed that the hard parton experiences a large number of soft scatterings with the medium, ($N_{\mathrm{scatt}} \gg 1$); the plasma is "thick". Gyulassy, Levai and Vitev (GLV) [119–123] took the Gyulassy-Wang model to another limit, that of the thin plasma ($N_{\mathrm{scatt}} \sim O(1)$). At this limit, the number of scattering amplitudes involved is still small enough for a brute force perturbative QCD calculation. This allows for complete treatment of all gluon and jet final state interactions, which is required to calculate the angular distribution of the radiation, $\frac{dN_g}{dyd^2\mathbf{k}_T}$ (where y is the rapidity).

In the GLV formalism the amplitude for radiating a gluon is constructed by summing up the relevant scattering amplitudes order by order in terms of the average number of scatterings per radiated gluon, $\langle N_{\mathrm{scatt}} \rangle = L/\lambda_g$, where λ_g is the mean free path of the gluon. As $\langle N_{\mathrm{scatt}} \rangle$ can be considered a measure of the medium opacity, this formalism is also known as "opacity expansion".

The first papers [119, 120] assumed an exclusive measurement of jet, gluon and recoil partons; in such an arrangement the exact number of participating scattering centers is known, as they are "tagged" via recoil particles. The qualitative results from these first studies suggested that while the angular distribution of radiated gluons was notably modified, the hard parton energy loss would actually be small.

The formalism was refined in later publications [121–123] which focused on the inclusive medium-induced gluon radiation, where the number of scattering centers participating in the radiation process fluctuates. In [121], a recursive formula for the opacity expansion of gluon radiation distribution was derived using the so-called "reaction operator". The graphs contributing to the radiation distribution at a particular order n of opacity were grouped in classes. For example, in the first order of opacity (one scattering center) there are contributions where one scattering is in the amplitude and one in its complex conjugate, but (in inclusive case) also terms with a double scattering in the amplitude and no scattering in the complex conjugate (or vice versa). Based on this classification, it is then possible to construct an operator which, given the single- and double-scattering combinations at order n, can build the gluon radiation distribution at order $n+1$ in opacity. This recursive method allows one to calculate the opacity expansion for the radiation to any order.

Interestingly, the result was that the first order of the opacity is dominating and thus it would be enough to assume a few scatterings for each radiated gluon. The size of the energy loss from medium-induced radiation was found to approach the BDMPS-Z result at RHIC energies [122]. Also the L^2 pathlength dependence could be obtained by assuming small effective formation probability for the radiation, $\gamma = \frac{L\mu^2}{4xE} \ll 1$, where x is the light cone momentum fraction carried by the radiated gluon.

GLV has been combined with longitudinally expanding Bjorken hydro [124] in a similar fashion as BDMS in the previous section. As the radiation intensity is inversely proportional to the mean free path of the radiated gluon ($\lambda_g^{-1} = n\sigma$) the scaling law was defined for the particle density in the medium, $n(\tau) = n_0 \left(\frac{\tau_0}{\tau}\right)^\alpha \theta(L-\tau)$. The energy loss by GLV is less than the BDMS result, but the difference diminishes towards higher jet energies. Also the effect of transverse flow v_T has been studied [125]. The conclusion was that while the strong transverse flow $v_T \sim 0.6$ would not have big effect on the overall magnitude of the jet quenching, the azimuthal asymmetry of the energy loss would be significantly reduced.

Later Djordjevic and Gyulassy [126] generalized the formalism to include also massive quarks; this version of the model is referred as DGLV. The energy loss for the heavy quarks was expected to be less than that of the light quarks due to the "dead cone" effect [127] which suppresses the forward radiation. The radiative heavy quark energy loss was seen to approach the incoherent (linear) limit in magnitude and pathlength dependence.

2.2.3 ASW

Gyulassy, Levai and Vitev were not the only ones studying the opacity expansion at the turn of the millennium. Wiedemann, who had earlier studied the opacity expansion for radiation in QED with Gyulassy [128], had independently developed another method to calculate the opacity expansion to nth order for QCD radiation [129, 130].

In [129], a non-abelian analogy for QED Furry approximation [131] was derived for the wavefunction of the high-energy parton. The Furry wavefunctions are solutions to Dirac equation with a series of static color potentials, and thus provide a very compact way to formulate the multiple-scattering problem. Armed with this formalism, Wiedemann derived in [130] a path integral representation for the gluon radiation cross section, valid for arbitrary (large) order in opacity. The result achieved in the leading order of $\frac{\omega}{E}$ agrees with Zakharov's, apart from the regularization scheme.

Together with Salgado, Wiedemann took his path integral expression for gluon radiation distribution $\frac{dI}{d\omega}$ to the single hard scattering limit, which agreed with the GLV result [132]. They also calculated the "quenching weights" – parton energy loss probability distributions – in both multiple soft and single hard scattering approximations. The approach was very similar to the previous studies of BDMS [133] and GLV [123]: The quenching weights are constructed by calculating Poissonian probabilities for N gluons removing a total energy ΔE from the high-energy parent parton. The average number of gluon emissions, which is required for Poissonian distribution, is obtained by integrating over $\frac{dI}{d\omega}$. Comparison between the multiple-soft and single-hard approximations revealed a rough agreement if the opacity $\langle N_{\mathrm{scatt}} \rangle$ is taken to be ≈ 3. An early application of the quenching weights in the calculation of the nuclear modification R_{AA} at

RHIC and the LHC can be found e.g. in Ref. [134].

These quenching weights were also calculated for an expanding medium modeled in a similar fashion as in BDMPS and GLV studies. For the single hard scattering, the medium effects were implemented in quenching weight calculation assuming the (longitudinal) density scaling $n(\tau) = n_0 \left(\frac{\tau_0}{\tau}\right)^{\alpha}$. For the multiple soft scattering, the scaled variable was the transport coefficient $\hat{q}(\tau) = \hat{q}_0 \left(\frac{\tau_0}{\tau}\right)^{\alpha}$, which represents the average transverse momentum squared transferred to the hard parton within the length of its mean free path. Approximate scaling laws were found, which relate the time-dependent parameters of expanding medium model to the time-independent versions in the static medium model. This allows for calculating the quenching weights for a dynamic medium in the effectively equivalent static scenario.

Massive quarks were added to the model by Armesto, Salgado and Wiedemann [135]; hence the formalism is known as ASW. While the "dead cone" was found to be filled by soft medium-induced gluon radiation, the quark mass reduces the higher-energy part of the radiation spectrum. Thus, as in DGLV, the radiative energy loss of heavy quarks was observed to be weaker than for the massless quarks.

2.3 AMY

The Gyulassy-Wang model and its successors BDMPS-Z, GLV and ASW were based on the assumption that the medium can be considered to be a collection of static scattering centers. This is a questionable presumption for the quark-gluon plasma, which is chiefly composed of light quarks and gluons and where the temperature, and therefore the average kinetic energy of the medium constituent, is of the order of a few hundred MeV. One formalism where static scattering centers are not used is by Arnold, Moore and Yaffe (AMY) [136–139]. They formulated a leading-order perturbative QCD (pQCD) hard thermal loop effective field theory treatment for the energy loss of a high-energy parton in a weakly coupled medium.

The AMY formalism is valid in the QCD plasma where the temperature T is high enough for the strong coupling to be actually weak, $g_s(T) \ll 1$. In the effective kinetic theory described in [139], the hard (quasi)particles traveling in this medium are assumed to have momentum of order T and thermal masses of the order $g_s T$ ($\ll T$ because of the weak coupling). The distributions $f(x, p)$ of these hard partons are evolved according to the Boltzmann equations of the form $(\partial_t + \mathbf{v} \cdot \nabla_{\mathbf{x}}) f(x, p) = -C[f]$, where $\mathbf{v}$ is the 3-velocity of a parton with 3-momentum $\mathbf{p}$ and C is the collision term.

The collision term can be split into two parts. One part contains the $2 \to 2$ -scatterings, calculated in leading order in pQCD, with the HTL self-energy contributions added where necessary. The other part features the medium-induced $1 \to 2$ -splittings, which, due to coherence, should be understood as

$N+1 \to N+2$ -processes. The splitting rates for $q \to qg$, $g \to q\bar{q}$, $g \to gg$ included in this part were calculated in [138]; in many of the later works [140–142], the "AMY formalism" usually means exactly these rates.

For soft scatterings with momentum transfer $q \sim O(g_s T)$, the mean free path is $\sim O(1/(g_s^2 T))$; this is also the scale for the radiation formation time. However, there can be also hard scatterings with $q \sim O(T)$. For these, the mean free path is $\sim O(1/(g_s^4 T))$. Thus, a large deflection to the parton direction can be caused by several soft scatterings or a single hard scattering. The small energy assumption $\omega \ll E$ for the radiated gluon used in the previous radiative studies is not made in this framework.

Together with longitudinally expanding Bjorken hydro, Turbide, Gale, Jeon and Moore [140] utilized the splitting rates from the above formalism to calculate the neutral pion modification factor and photon production in RHIC central collisions. The original Bjorken hydro model was slightly modified to take account the nonuniform transverse density profile due to finite transverse nuclear radius R_T in initial temperatures: $T(r,\tau) = T_i \left(\frac{\tau_0}{\tau}\right)^{1/3} \left[2\left(1 - \frac{r^2}{R_T^2}\right)\right]^{1/4}$. Likewise, the initial transverse positions of the hard partons were distributed using the hard sphere profile $P(\mathbf{r}_T) = \frac{2}{\pi R_T^2}\left(1 - \frac{r_T^2}{R_T^2}\right)\theta(R_T - r_T)$.

The ending condition for the evolution of the hard parton distributions was $T = 160$ MeV, while two scenarios were studied for initial time and temperature: $T_i = 447$ MeV with $\tau_0 = 0.147$ fm and $T_i = 370$ MeV with $\tau_0 = 0.26$ fm. A constant strong coupling value $\alpha_s = 0.3$ gave a good agreement with the measured $R_{AA}^{\pi^0}(p_T)$ in both scenarios. From this, the conclusion was made that for the energy loss, the duration of the hard parton evolution is more crucial parameter than the initial temperature. A prediction for the LHC was also made; it was expected that the overall suppression would increase by a factor of 2 for a 10 GeV pion and $R_{AA}(P_T)$ would rise very slowly between 5 to 30 GeV. As was mentioned in Chapter 1, it is now known that this prediction did not come true; there is only roughly 20% increase in the suppression, while $R_{AA}(P_T)$ in fact rises quite steeply from 7 to 20 GeV.

Later Qin, Ruppert, Gale, Jeon, Moore and Mustafa [141] compared the energy loss by AMY radiation and elastic collisions. While the radiative suppression was found to be approximately 1.5 times larger, the elastic energy loss was nevertheless notable: For a 10 GeV neutral pion, $R_{AA} \approx 0.55$ with purely collisional energy loss in central collisions at RHIC.

2.4 Higher twist

The theoretical treatment of proton-proton and nucleus-nucleus collisions rests strongly on the so-called factorization theorem, which is discussed in more detail in Chapter 3. The basic idea is that the problem of producing hadrons in hadronic scattering processes can be divided into three parts: The non-

perturbative parton distribution functions (partons from hadrons), the perturbative partonic scattering cross section and finally the non-perturbative fragmentation functions (hadrons from partons). All the energy loss models above concentrate on calculating medium corrections on the partonic middle part where the full pQCD arsenal is available. In the higher twist (HT) energy loss formalism, the medium modification is implemented into the energy scale evolution of the fragmentation functions. It was developed first in the early '90s by Luo, Qiu and Sterman [77–79], later in 2000s by Wang *et al.* [80, 81] and recently also by Majumder *et al.* [82–85].

In the deep inelastic scattering, the forward photon-proton scattering amplitude can be expanded as a product of particle current operators. This expansion is ordered by the difference of the dimension and the spin, or *twist*, of the operators. Given a virtual photon energy scale Q, the contribution from an operator with a twist t is suppressed by a factor of $(1/Q)^{t-2}$. In QCD, the twist is directly proportional to the particle field correlations; twist-2 operator corresponds to correlation functions of two fields etc. The important finding of Luo, Qiu and Sterman was that certain higher-twist corrections are enhanced in a nucleus, the enhancement being proportional to nuclear radius $R_A \sim A^{1/3}$ [77]. Later Wang and Guo showed that the LPM effect further increases this dependence to R_A^2 [81].

The higher-twist ($t \geq 4$) corrections are implemented into the factorization theorem by modifying the DGLAP (Dokshitzer [143], Gribov and Lipatov [144], Altarelli and Parisi [145]) evolution equations of the fragmentation function of the high-energy parton. This modification contains twist-4 parton matrix elements which describe the additional scattering of the hard parton with another nucleon inside the nucleus. The model involves one free parameter $\tilde{C}$ which is related to the quark-gluon correlation strength inside nuclei and must be fixed by a fit to the experimental data. In later studies this parameter was redefined as the jet transport coefficient $\hat{q}$, mentioned in the ASW section.

As the fragmentation functions are present from the beginning, this model does not assume on-shell partons at any point during the evolution. In many ways, this approach is thus complementary to the AMY formalism, which has a detailed description of partonic interactions but on the other hand no vacuum radiation, which is inherent in HT. Also the medium in AMY is for all intents and purposes infinite, while the higher twist works best with a thin medium.

These differences show up in nuclear modification level: While $R_{AA}(P_T)$ for high-energy neutral pions at RHIC is flat for AMY, the early HT prediction by Wang and Wang showed a rising trend [146]. In both cases, the simple longitudinally expanding hydro was (once again) used to model the medium; for higher twist, as with GLV above, the particle density was the time-dependent parameter. However, this prediction of rising R_{AA} was not supported by the later PHENIX data [147].

The subsequent studies [148–150] have reached an agreement not only with RHIC R_{AA}, but also with the nuclear modification in the LHC. In each of these,

the medium evolution and initial profile was connected to energy loss in a different way: In [148], the transport coefficient $\hat{q}(\tau, \mathbf{r})$ depended on transverse density of the number of participants $n_{\mathrm{part}}(\mathbf{b}, \mathbf{r})$ ($\mathbf{b}$ being the impact parameter) and was inversely proportional to τ; in [149] it was determined by medium flow and parton and hadron densities (which varied in time and position); and in [150], it scaled with space-time dependent entropy density.

2.5 Modern elastic energy loss models

The interest in elastic energy loss was reawakened in the 2000s with heavy flavor results from RHIC [151, 152]. As mentioned above, the dead cone effect associated with massive quarks was expected to reduce the energy loss compared to the light quarks. However, according to the experimental results, the heavy flavor energy loss was in fact comparable with the light flavors. This raised the question whether the size of the collisional energy loss had been underestimated in the earlier studies.

Mustafa and Thoma [153] had already been studying light partons undergoing Brownian motion in a medium with longitudinal Bjorken expansion, based on the energy loss calculations by Thoma a decade earlier [154]. Their finding was that in such a setting, the collisional and radiative quenching factors are of similar magnitude. Mustafa then proceeded to include charm quarks in the formalism [155], ending up with similar conclusions as with the light quarks.

Conversely, Dutt-Mazumder, Alam, Roy and Sinha [156] took the heavy fermion calculations of Braaten and Thoma as a starting point to calculate the light parton collisional energy loss per unit length $\frac{dE}{dx}$ in a static medium. Their analysis accounted for most leading-order pQCD $2 \to 2$ processes; the ignored ones were $q_i\bar{q}_i \to q_j\bar{q}_j$ in a quark case and $gg \to q\bar{q}$ in a gluon case. In a static, constant-temperature medium the collisional energy loss was found to be even larger than radiative up to parton energies $\sim 60 - 70$ GeV.

Wicks, Horowitz, Djordjevic and Gyulassy [157] extended the DGLV formalism to include also the elastic energy loss, using both Thoma-Gyulassy and Braaten-Thoma calculations to map out uncertainties. Fluctuations around the average elastic energy loss value were introduced by Gaussian distribution with variance $2T$ times the average. Also the hard parton pathlength L was varied using Woods-Saxon nuclear density profile. Bjorken longitudinal expansion was then taken into account by calculating the medium density at the average time $\tau = L/2$. Also this study came to the conclusion that the elastic energy loss cannot be neglected. Later comparison of the WHDG elastic+radiative model with the LHC data for charged hadron $R_{AA}(P_T)$ showed some qualitative agreement, but the amount of suppression was overestimated [158].

In relation to the above WHDG study, Djordjevic [159] investigated the finite size effects on Thoma-Gyulassy and Braaten-Thoma results by calculating the collisional energy loss "up to a zeroth order in opacity" in a static medium,

which in practice means calculating $2 \to 2$ -process with an effective HTL gluon propagator. The finite size effects were found to have little effect, providing support for the WHDG result. As an useful side product, an improved calculation of the infinite medium elastic energy loss was obtained.

Wang [160] and Majumder [161] utilized the higher twist formalism also for elastic energy loss calculations. Wang found an interference between elastic and radiative amplitudes which reduced elastic energy loss at small propagation lengths $< 1 - 2$ fm, which would affect the centrality dependence of elastic energy loss. Majumder focused on those processes which did not interfere with the radiative amplitudes; his results for average elastic energy loss per unit length were of same size as Braaten-Thoma and Djordjevic.

In all the above models, the strong coupling constant was fixed. Gossiaux, Aichelin and collaborators [162–164] have studied the elastic energy loss of heavy quarks with the running coupling constant $\alpha_s(Q^2)$ [165] extended to space-like sector $Q^2 < 0$. Using the Boltzmann equation formalism and the (2+1)-D hydrodynamical model by Kolb and Heinz [166], their model managed to reach a reasonable agreement with both $R_{AA}(P_T)$ and $v_2(P_T)$ of the heavy flavors in RHIC with a normalization factor $K \approx 2$. This would imply that the elastic and radiative energy loss components are of roughly the same size for heavy quarks.

2.6 Energy loss in Monte Carlo simulations

It is safe to say that most of the Monte Carlo (MC) implementations of the in-medium shower evolution are based on *the* Monte Carlo simulation in the field of particle physics, PYTHIA [167, 168]. This is somewhat natural, as PYTHIA is widely used in experimental data analysis and thus it offers a well tested baseline for energy loss model-building. It has two parts: the virtuality-ordered partonic shower and the hadronic string fragmentation.

The PYTHIA parton shower is based on iterating the $1 \to 2$ splitting. The probability for the splitting of parton a between initial and final virtuality scales Q_i, Q_f is governed by the Sudakov form factor

$$S_a(Q_i^2, Q_f^2) = \exp\left(- \int_{Q_i^2}^{Q_f^2} \frac{dQ'}{Q'^2} \int dz \frac{\alpha_s(k_T^2)}{2\pi} \sum_b P_{ab}(z) \right), \qquad (2.1)$$

where P_{ab} is the splitting function for a parton b to take a momentum fraction z in a process $a \to b + c$ and the running coupling is evaluated at the transverse momentum of the splitting ($k_T^2 \simeq (1-z)Q'^2$ for initial state and $k_T^2 \simeq z(1-z)Q'^2$ for final state splitting).

After the parton shower evolution has ended, the system must be hadronized. Thus an important component of PYTHIA is the Lund string fragmentation [169], where the quark-antiquark pairs produced in nucleon-nucleon collisions are connected with strings. If gluons are also produced, they will form "kinks"

on the strings. If there is sufficient energy stored in the string, a new quark-antiquark pair can be formed which breaks the string. If these pieces still contain enough energy, they can further break into smaller bits until they equal hadrons on their mass shells.

2.6.1 HIJING

One of the earliest Monte Carlo approaches to heavy ion collision modeling was HIJING [170] (Heavy Ion Jet INteraction Generator), developed by Wang and Gyulassy in the beginning of 1990s. It already contained some subroutines of PYTHIA and also a schematic energy loss model for medium-induced radiation, based on a simple gluon splitting mechanism. The interaction points were determined by the probability $dP = \frac{dl}{\lambda_s} e^{-l/\lambda_s}$, l being the distance traveled by the jet and λ_s denoting the mean free path. In each interaction point, collinear gluon splitting was performed and part of the parton energy was transferred from one Lund string configuration to another. The simulation results predicted a substantial ($\sim$ factor 3) suppression for charged particles with $P_T > 4$ GeV in Au+Au collisions at $\sqrt{s_{NN}} = 200$ GeV.

2.6.2 HYDJET/HYDJET++ and PYQUEN

First of the present-day Monte Carlo simulations to be introduced is by Lokhtin, Snigirev *et al.*. HYDJET (HYDrodynamics plus JETs) written in Fortran, and HYDJET++, written in C++, model the heavy ion collisions by modifying a standard PYTHIA event. The simulation is divided into "soft" part with flow effects and "hard" part where the hard jets are modified with PYQUEN (PYthia QUENched) [86, 87].

Both radiative and collisional energy losses are included in PYQUEN, and the hard parton suffers both kinds of energy losses at each scattering. The additional radiation is produced according to the BDMS spectrum [171, 172], while the elastic energy loss is calculated using the dominant (t-channel) contribution to the scattering cross section σ. Running coupling $\alpha_s(Q^2)$ is included; for radiative calculation, the relevant energy scale is $Q^2 = \mu_D^2$, while for collisional it is $Q^2 = t$. The distance between successive scatterings is sampled according to the mean free path $\lambda = (\sigma(\tau)\rho(\tau))^{-1}$, the time evolution of the medium being modeled by the standard Bjorken hydro with 1-D evolution.

The tuning parameters of the model are the K-factor, used in the calculation of jet production cross section to take into account the higher-order pQCD corrections; number of active quark flavors N_f; formation time τ_0, initial temperature T_0 and freeze-out temperature T_f; maximum transverse flow rapidity Y_{max} and minimum transverse momentum transfer p_{Tmin} in a hard scattering. After fixing these parameters by fitting the PHENIX neutral pion P_T spectra, the model reproduces quite nicely the RHIC results for charged hadron pseudorapidity distributions for various centralities and also the azimuthal two-particle

correlation function for central collisions.

2.6.3 Q-PYTHIA

As the name suggests, Q-PYTHIA [88] by Armesto, Cunqueiro and Salgado, is PYTHIA with modified routine for virtuality-ordered final state radiation. As the total radiation spectrum is a sum of vacuum and medium terms, $dI^{\text{tot}} = dI^{\text{vac}} + dI^{\text{med}}$, and the vacuum term is associated with the splitting function $P(z)$ by $\frac{dI^{\text{vac}}}{dz d\mathbf{p}_T^2} = \frac{\alpha_s}{2\pi \mathbf{p}_T^2} P(z)$, the modification is done by adding a medium correction term to the vacuum splitting functions: $P_{\text{tot}}(z) = P(z) + \Delta P(z, Q, \hat{q}, L, E)$. The medium-induced gluon radiation spectrum is modeled according to the BDMPS, and depends on the virtuality Q and energy E of the radiating parton, the transport coefficient $\hat{q}$ and length of the medium L (which will be modified on each iteration by the formation time τ_f required before next splitting: $L_n = L_{n-1} - \tau_f$). In the first comparisons with RHIC data, the compatibility between Q-PYTHIA and experimental results has been rather poor, however [173].

2.6.4 JEWEL

JEWEL (Jet Evolution With Energy Loss) by Zapp *et al.* [89, 90] produces in vacuum a parton shower which mimics that of PYTHIA described above, and the hadronization is executed with the Lund string fragmentation routine of the latter. The medium is modeled as an ideal gas of quarks and gluons at temperature T. A parton shower is evolved through the medium, experiencing both vacuum-like splittings and $2 \to 2$ scatterings with the medium.

The probability for no $2 \to 2$ scattering is $\exp\left(-\int_{\tau_i}^{\tau_f} \sigma_{2\to2}(\zeta) n(\zeta) d\zeta\right)$, where ζ represents the trajectory of the hard parton. The t-channel cross section $\sigma_{2\to2}$ is evaluated at the running coupling scale $|t| + \mu_D^2$ with the Debye mass $\mu_D \approx 3T$. The density of the medium constituents is n. The initial time τ_i is the time of previous splitting or scattering, while $\tau_f = \frac{E}{Q^2}$ is the lifetime determined by the virtuality Q and energy E of the hard parton. On-shell partons may scatter until they exit the medium.

The latest version of JEWEL [90] includes an implementation of the LPM effect. This is done in the style of BDMPS, where transverse momentum "kicks" received from the elastic scatterings modify the formation time of the radiated gluon [174,175]. If the formation of the gluon is not completed within the limits of the medium, it is rejected.

Using the Glauber model for initial density profile and evolving the medium with the Bjorken hydro, with critical temperature $T_C = 165$ MeV, initial temperature $T_i = 350$ MeV and initial time $\tau_i = 0.8$ fm, JEWEL produces roughly the right amount of the high-P_T neutral pion R_{AA} in central collisions at RHIC [90]. Utilizing the relation $dN/dy \propto \tau_i T_i^3$, the initial temperature for the quark-gluon plasma in the LHC is derived using RHIC values using the measured

charged hadron multiplicities: $T_i^{\rm LHC} = T_i^{\rm RHIC}\left(\frac{\tau_i^{\rm RHIC}}{\tau_i^{\rm LHC}}\frac{dN/dy|_{\rm LHC}}{dN/dy|_{\rm RHIC}}\right)^{1/3}$. With the values $T_i = 530$ MeV and $\tau_i = 0.5$ fm for the LHC, JEWEL reaches quite good agreement with the preliminary charged hadron $R_{AA}(P_T)$ data from ALICE and CMS.

2.6.5 YAJEM

Yet another Jet Energy-loss Model (YAJEM) by Renk [91–94], modifies the PYTHIA parton shower in a style which is phenomenologically similar to JEWEL above. Here interactions with the medium increase the virtuality of a shower parton by an amount $\Delta Q_a^2 = \int_{\tau_a^0}^{\tau_a^0+\tau_a} \hat{q}(\zeta)d\zeta$, where τ_0^a is the production time of the parton a and τ_a its lifetime, sampled from a probability distribution $P(\tau_a) = \exp\left(-\tau_a/\langle\tau_a\rangle\right)$, $\langle\tau_a\rangle$ being the average lifetime estimated from the virtuality and energy of the parton. The parton trajectory is again represented by ζ, and $\hat{q}$ is the transport coefficient. It can be further expressed as [176, 177]

$$\hat{q}(\zeta) = 2K[\epsilon(\zeta)]^{(3/4)}[\cosh\rho(\zeta) - \sinh\rho(\zeta)\cos(\psi)],$$

where K is the interaction strength parameter, ϵ is the energy density of the medium, ρ is the local flow rapidity and ψ the angle between parton trajectory and the flow. In principle, $\hat{q}$ thus contains all the information about the medium properties and the energy loss.

In the case of large virtuality increases, the virtuality-dependent average lifetime of the parton $\langle\tau_a\rangle$ will change notably. In such cases, the calculations of $\langle\tau_a\rangle$ and ΔQ_a are iterated to determine a self-consistent pair ($\langle\tau_a\rangle$,ΔQ_a). This procedure accounts for the LPM effect.

It is to be noted that in this basic setup, the parton shower actually *gains* energy from the medium as the energy transfers *to* the medium are not modeled. However, due to the radiation induced by the increased virtuality, the energy within the shower is transferred from the hard partons to the soft radiation, producing the suppression of high-energy hadrons (assembled by the Lund string fragmentation) as the end result.

A straightforward energy loss can be implemented by introducing a drag coefficient $\hat{e}(\zeta)$, defined analogously with the transport coefficient $\hat{q}$. Energy loss is then $\Delta E_a = \int_{\tau_a^0}^{\tau_a^0+\tau_a} \hat{e}(\zeta)d\zeta$ [92]. This corresponds to elastic energy loss, while the virtuality modification is related to the radiative energy loss. Thus comparisons between elastic and radiative suppression can be made; the STAR dihadron data supports roughly 10% elastic contribution [178].

Using a pathlength-dependent minimum virtuality scale $Q_0 = \sqrt{E/L}$ and (3+1)-D hydro [179], YAJEM succeeds in reproducing the PHENIX in-plane/out-of-plane variation of $R_{AA}(P_T, \phi)$ for 20-30% centrality [94]. In a separate study with (2+1)-D hydro, quite good agreement was achieved also with the LHC charged hadron $R_{AA}(P_T)$ [180].

2.6.6 MARTINI

The event generator MARTINI (Modular Algorithm for Relativistic Treatment of heavy IoN Interactions) by Schenke *et al.* [181] uses PYTHIA to generate the hard partons from the individual nucleon-nucleon collisions and to take care of the final fragmentation into hadrons. The vacuum shower is included up to the beginning of the hadronic phase. There are no interference effects between the vacuum shower and the medium.

For jet-medium interactions, the McGill-AMY parton-evolution formalism [141,182] is used. In this formalism, the evolution is governed by a set of coupled Fokker-Planck-type rate equations. Both elastic and radiative transition rates are calculated in perturbative QCD; the former utilizes the t-channel scattering amplitudes and Bose-Einstein/Fermi-Dirac thermal distributions [142], while for the latter the AMY results are used. Also included are the quark-gluon and gluon-quark conversions, photon radiation (calculated analogously with gluon radiation) and jet-photon conversions.

The flow of the medium adds the requirement of Lorentz boosts into the rest frame of the fluid cell before calculating the (temperature-dependent) transition rates. The probability for medium interaction in a time step Δt is given by the sum of all possible transition rates, multiplied by Δt. In the case of interaction, the process to take place is determined by the relative weights of the possible processes. In the end, the parton is boosted back to the laboratory frame and the system moves to the next time step. All partons, including the radiated ones, are followed as long as their energy is above $4T$.

Using (2+1)-D hydro [166, 183, 184] with a fixed strong coupling $\alpha_s = 0.33$ or, alternatively, (3+1)-D hydro [179] with $\alpha_s = 0.3$, MARTINI gives the right amount of suppression for neutral pions at RHIC, both in 0-10% and 20-30% centralities. However, (3+1)-D hydro is needed to reproduce the separation of in-plane and out-of-plane $R_{AA}^{\pi^0}(P_T, \phi)$ in the 20-30% centrality class. Combined with (3+1)-D hydro MUSIC [185], MARTINI reproduces quite well the dijet asymmetry measured in the LHC Pb+Pb collisions [186].

2.6.7 BAMPS

While most of the Monte Carlo models concentrate on simulating the high-energy part of the particle spectrum, BAMPS (Boltzmann Approach of MultiParton Scatterings) by Xu, Greiner *et al.* [187–190] attempts to include everything within one framework. It is an example of a parton cascade model (PCM); other, slightly older representatives of PCMs are ZPC [191], MPC [192], PCPC [193] and VNI/BMS [194].

All partons are treated as semiclassical, on-shell particles evolved by the Boltzmann equations. The initial momentum distribution of the partons is determined by the differential jet cross sections of a nucleon-nucleon collision. The initial position distribution is according to the Glauber geometry.

The probabilities for $2 \to 2$ processes are dictated by their leading-order pQCD cross sections in the t-channel approximation. The calculation of $2 \to 3$ (and $3 \to 2$) -processes is based on the effective Gunion-Bertsch matrix element [103], which factorizes into collisional and radiative parts: $|M_{GB}|^2 = |M_{\rm coll}|^2 P_g$. The LPM effect is implemented by requiring that the formation time of the radiation is smaller than the mean free path of the radiating parton. This requirement leads to a cutoff on the lower limit of the transverse momentum of the radiated gluon. In areas with energy density below the freeze-out value ϵ_C, the particles propagate freely. Hadronization is done with fragmentation functions.

With a strong coupling value $\alpha_s = 0.3$ and freeze-out density $\epsilon_C = 0.6$ GeV/fm^3, the p_T-integrated v_2 produced by BAMPS agrees with RHIC results [195]. However, the differential $v_2(p_T)$ is underestimated in the model, and the suppression of high-energy hadrons is strongly overpredicted [196]. The problem persists to the LHC energies. On the other hand, the heavy flavor calculations using just elastic interactions and the running coupling do achieve a rough agreement for both $v_2(p_T)$ and $R_{AA}(p_T)$ at RHIC simultaneously, when the interaction cross section is multiplied by 4 to emulate radiative contribution [190].

2.6.8 Monte Carlo model of this thesis

The Monte Carlo model for a purely elastic energy loss [I], the subject of this thesis, has been developed concurrently with the other modern MC models such as JEWEL, YAJEM and MARTINI. Many of the models described in this Chapter possess highly advanced formalisms, which are hard to control or combine with modern, sophisticated models for the hydrodynamical medium. For this reason, the aim has been to develop an energy loss model, which is based on rigorous pQCD calculations, has simple control parameters (which prove to be the strong coupling constant α_s and the thermal mass magnitude parameter s_m) and which can easily utilize the modern hydro models that have been tested against the experimental data. The model thus provides a solid baseline calculation, on which the more complicated concepts (such as coherence effects) can be added in the future. Here, a brief summary of the operation of the simulation is given; a more detailed look is provided in the next Chapter.

The hard parton is propagated through the medium in small time steps Δt. The collision probability at each time step is based on the Poissonian distribution $e^{-\Gamma \Delta t}$, where $\Gamma(E,T) = \lambda^{-1}$ is the scattering rate of the hard parton with energy E in a medium with temperature T. The temperature – and the 3-dimensional flow of the medium, which is also taken into account by default – at each spacetime point is obtained from the hydrodynamical model in use. The Monte Carlo model itself assumes as little as possible about the medium; the postulate is that it consists of massless quarks and gluons which respect either the Fermi-Dirac (quarks) or the Bose-Einstein (gluons) thermal distribution.

The scattering processes are controlled by the full leading-order pQCD $2 \to 2$ scattering amplitudes and the rigorous conservation of energy and momentum. Unlike in most of the models discussed above, no extra assumptions are made about the relative energies of the hard parton and the thermal particle, or the momentum transfer between them; the high-energy particle can and will change its direction in the scatterings, and the parton with the higher energy in the initial state of the scattering does not necessarily have higher energy in the final state, leading to the possibility for a change of identity for the followed hard parton, as only the leading parton energy loss is modeled here. This is not necessary, however: Having a full information of both final state particles enables equal treatment for both the hard parton and the recoil particle.

The simulation ends when the temperature has reached a low enough value for the system to be considered to have entered the hadronic phase. The procedure is then repeated for several thousands of partons, which produces a momentum distribution of the hard parton. This distribution is then convoluted with the fragmentation functions in order to arrive at a hadron spectrum, which can be compared with the experimental data. The results obtained by utilizing various hydrodynamical setups are described in Chapter 4; as already seen above in the case of BAMPS, for example, it is found to be crucial to compare the model simultaneously against several different observables.

Chapter 3

Monte Carlo modeling of elastic energy loss

As already seen in Chapter 2, there are several different physics aspects related to the heavy ion collisions, which must be taken into account in the energy loss models. The very first issue is the geometry of a nuclear collision; how large portion of the nucleons inside the two colliding nuclei actually participate in the collision? The answer to this affects not only the starting point distributions for the hard parton, but also the energy densities and the shape of the (possibly) forming medium. There is also the question of the medium itself; what determines its dynamics, how does it form in the first place, and what happens at the end of the evolution?

Correct treatment of the high-energy parton, for which the energy loss is calculated, is not a simple matter either, starting from how it is produced and what are its initial momentum and flavor. Specifying the interactions between the hard parton and the medium is the central point of any energy loss model; numerous ways to handle this were described in the previous Chapter. At the end, the parton must yet be converted to hadrons.

This Chapter briefly describes how these problems can be handled at the theoretical level, and how the theory is implemented in the Monte Carlo simulation of this thesis.

3.1 Nuclear collision geometry

3.1.1 Optical Glauber model

As explained in the Introduction, a nucleus consists of nucleons (protons and neutrons). To predict the produced particle spectra in nucleus-nucleus $(A + B)$ collision events, one must estimate the number of nucleon-nucleon $(N + N)$ collisions in one such event.

One can begin by examining the proton-nucleus $(p + A)$ collision. The proton hits the nucleus at an impact parameter $\mathbf{b}$, which measures the transverse

distance from the center of the nucleus. Knowing the inelastic cross section $\sigma_{NN}(\sqrt{s_{NN}})$ for a nucleon-nucleon collision at a center-of-mass energy $\sqrt{s_{NN}}$, the average number of binary nucleon-nucleon collisions in a $p+A$ collision event is

$$N_{\rm bin}^{pA}(\mathbf{b}) = T_A(\mathbf{b})\sigma_{NN}(\sqrt{s_{NN}}), \tag{3.1}$$

where the nuclear thickness function $T_A(\mathbf{b})$ is defined as

$$T_A(\mathbf{b}, z) = \int_{-\infty}^{\infty} dz\, \rho_A(\mathbf{b}, z). \tag{3.2}$$

The nuclear density $\rho_A(\mathbf{b})$ is given by the Woods-Saxon distribution [197]

$$\rho_A(\mathbf{b}, z) = \frac{\rho_0}{\exp\frac{r-R_A}{d} + 1}, \tag{3.3}$$

with $r = \sqrt{|\mathbf{b}|^2 + z^2}$ and $R_A = 1.12A^{1/3} - 0.86A^{-1/3}$. The values of the nuclear thickness d and the central density ρ_0 must fulfill the normalization condition

$$\int d^2\mathbf{b}\, T_A(\mathbf{b}) = A. \tag{3.4}$$

For RHIC Au-Au -collisions, the nuclear thickness is $d = 0.54$ fm and $\rho_0 = 0.17$ fm^{-3}.

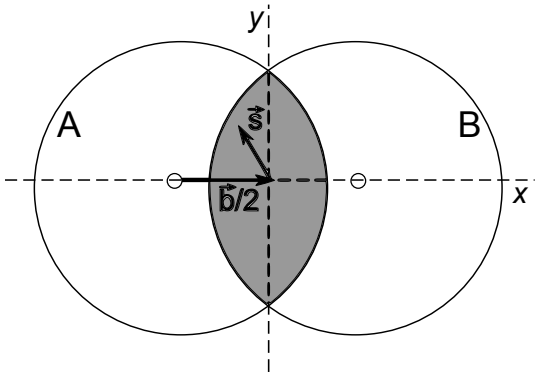

Figure 3.1: Two overlapping nuclei in the transverse plane. The vector $\mathbf{b}$ is the impact parameter.

The generalization of $p + A$ to $A + A$ is done by defining the nuclear overlap function T_{AB},

$$T_{AB}(\mathbf{b}) = \int d^2\mathbf{s}\, T_A(\mathbf{s} + \mathbf{b}/2)T_B(\mathbf{s} - \mathbf{b}/2), \tag{3.5}$$

with the normalization

$$\int d^2\mathbf{b}\, T_{AB}(\mathbf{b}) = AB, \tag{3.6}$$

and the orientation of vectors $\mathbf{s}, \mathbf{b}$ as in Fig. 3.1. The average number of binary nucleon-nucleon collisions in the nucleus-nucleus collision with impact parameter $\mathbf{b}$ is then

$$N_{\rm bin}^{AB}(\mathbf{b}) = T_{AB}(\mathbf{b})\sigma_{NN}(\sqrt{s_{NN}}). \tag{3.7}$$

Assuming all $N+N$ collisions to be independent, and $AB \gg 1$, one can then formulate the inelastic cross section of the $A+B$ collision as

$$\begin{aligned}\sigma_{\rm inel}^{AB} &= \int d^2\mathbf{b}\left(1-\left(1-\frac{T_{AB}(\mathbf{b})\sigma_{\rm inel}^{NN}}{AB}\right)^{AB}\right) \\ &\underset{AB\gg 1}{\approx} \int d^2\mathbf{b}\left(1-e^{-T_{AB}(\mathbf{b})\sigma_{\rm inel}^{NN}}\right).\end{aligned} \tag{3.8}$$

This result is known as the *optical Glauber model* [198].

Another important number that can be derived from the collision geometry is the number of participants (or "wounded nucleons") $N_{\rm part}$. Considering a nucleon from the nucleus A, its probability to *not* collide with any of the nucleons from the nucleus B is

$$P = \left(1-\frac{\sigma_{NN}T_B(\mathbf{s}-\mathbf{b}/2)}{B}\right)^B \underset{B\gg 1}{\approx} e^{-\sigma_{NN}T_B(\mathbf{s}-\mathbf{b}/2)}. \tag{3.9}$$

Thus the number of participants – the nucleons with at least one interaction – from the nucleus A is

$$N_{\rm part}^{A} = \int d^2\mathbf{s} T_A(\mathbf{s}+\mathbf{b}/2)\left(1-e^{-\sigma_{NN}T_B(\mathbf{s}-\mathbf{b}/2)}\right), \tag{3.10}$$

and the total number of participants from both nuclei is

$$\begin{aligned}N_{\rm part}^{AB} = \int d^2\mathbf{s}\Big(&T_A(\mathbf{s}+\mathbf{b}/2)\left(1-e^{-\sigma_{NN}T_B(\mathbf{s}-\mathbf{b}/2)}\right) \\ &+T_B(\mathbf{s}-\mathbf{b}/2)\left(1-e^{-\sigma_{NN}T_A(\mathbf{s}+\mathbf{b}/2)}\right)\Big).\end{aligned} \tag{3.11}$$

3.1.2 Monte Carlo Glauber model

The Monte Carlo Glauber method [198] is a natural way to study single events for event-by-event hydrodynamics such as [199], utilized in the paper [IV] of this thesis. Here the nucleon positions inside the nuclei are generated randomly, using the Woods-Saxon distribution (3.3) as a probability weight function. After the nucleon distribution for both colliding nuclei has been created, the impact parameter is sampled from the distribution $\frac{dN}{db} \sim b$. Distances between two nucleons from the different nuclei are calculated; if this distance is less than $\sqrt{\sigma_{NN}/\pi}$, the nucleons are assumed to interact. When all pairs have been considered, the number of binary collisions and wounded nucleons in this particular collision event is known.

3.1.3 Centrality classes

The Glauber model is needed for grouping the collision events into different *centrality classes*. Knowing the inelastic cross section distribution as a function of the impact parameter (squared), $\frac{d\sigma_{\rm inel}^{AA}}{db^2}$, the portion of $X\%$ most central collisions in the optical Glauber model is

$$\frac{X}{100}\sigma_{\rm inel}^{AA} = \pi \int_0^{b^2(X\%)} db^2 \left(1 - e^{-T_{AA}(\mathbf{b})\sigma_{\rm inel}^{NN}}\right), \tag{3.12}$$

which fixes the impact parameter intervals $[0, b(X\%)]$ for each centrality class. For the Monte Carlo Glauber, the procedure is analogous, but instead of the impact parameter, the number of participants or binary collisions is used.

However, the impact parameter of an event cannot be directly measured in experiments. Instead one measures the number of charged particles $N_{\rm ch}$ in different directions. Many particles in the direction of the beam axis (remnants of the nuclei) and few particles in transverse direction (particles produced in the collision) implies large $\mathbf{b}$; conversely, high number of particles transverse to the beam axis and few in the beam direction suggests impact parameter closer to zero.

Ideally, the charged particle multiplicity per event $dN/dN_{\rm ch}$ would be measured for a large number of events and this distribution would be binned in fractions of the total number of events. This is then compared with Glauber calculations to obtain the mean impact parameter $\langle b(X\%)\rangle$ or number of participants $\langle N_{\rm part}(X\%)\rangle$ for a certain centrality class $X\%$. In practice, the analysis is complicated by the experimental uncertainties and natural statistical fluctuations around the mean values.

3.1.4 Glauber model implementation in this thesis

From the integrand of T_{AB} (3.5), the initial starting point $(x_0, y_0) = \mathbf{s}_0$ of the hard parton can be determined using the hit-or-miss procedure: The points x_0 and y_0 are picked randomly from the transverse plane[1]. In addition, a third random number R is picked from the interval $R \in [0, T_A(\mathbf{b}/2)T_B(-\mathbf{b}/2)]$. If $T_A(\mathbf{s}_0 + \mathbf{b}/2)T_B(\mathbf{s}_0 - \mathbf{b}/2) \geq R$, the point (x_0, y_0) is accepted; otherwise, a new set of random numbers $\{x_0, y_0, R\}$ is chosen. The centrality class is taken into account by using the appropriate average impact parameter $\langle b(X\%)\rangle$.

In the event-by-event elastic energy loss simulations, presented in Paper [IV], the initial starting points of the hard partons are randomly selected from the list of binary collision vertices provided by the hydrodynamic simulation for each event.

[1]To be exact, the transverse plane is represented as a discrete grid, so that a table of thickness function values can be used instead of doing the integrations at every evaluation. However, the spacing of the grid is kept very small, $\sim O(0.01)$ fm.

3.2 Hydrodynamical background

When studying the interactions of a particle with a medium, one important issue is the modeling of the medium. There are basically two approaches: microscopical and macroscopical. In the microscopical approach, one models the medium as a collection of individual particles (such as quarks and gluons) interacting with each other. BAMPS, and the other parton cascade models mentioned in Chapter 2, are examples of this approach. However, in the macroscopical approach – which is the one applied in this thesis – one treats the medium as a continuous fluid in a local thermal equilibrium (or at least close to it). The spacetime evolution of this fluid is governed by the hydrodynamical equations; the connection to the microscopic properties of the system is provided by the Equation of State (EoS)[2].

3.2.1 Hydrodynamical equations

The hydrodynamical equations of motion applied in the present work are obtained by requiring local conservation of energy and momentum of the bulk fluid, given by the energy-momentum tensor $T^{\mu\nu}$, and baryon-number currents j_i^μ:

$$\begin{aligned} \partial_\mu T^{\mu\nu} &= 0 \\ \partial_\mu j_i^\mu &= 0. \end{aligned} \tag{3.13}$$

If an ideal fluid is assumed, the energy-momentum tensor contains no dissipative terms and can be written as

$$T^{\mu\nu} = [\epsilon(x) + p(x)]\, u^\mu(x) u^\nu(x) - p(x) g^{\mu\nu}, \tag{3.14}$$

where $\epsilon(x)$ is the energy density, $p(x)$ is the pressure and $u^\mu(x) = \gamma(1, v_x, v_y, v_z)$, with 3-velocity components v_x, v_y, v_z and the Lorentz gamma factor $\gamma = 1/\sqrt{1-v^2}$, is the fluid 4-velocity. Also, if the charge density in the local rest frame of the fluid is $n_i(x)$, the charge current in the global reference frame is now $j_i^\mu(x) = n_i(x) u^\mu$.

If longitudinal boost-invariance at spatial midrapidity[3], $\eta = \frac{1}{2}\log\frac{t+z}{t-z} \approx 0$, is assumed together with a longitudinal scaling flow $v_z = \frac{z}{t}$, it follows that if the thermodynamical variables are independent of rapidity at the initial proper time τ_0, they will not develop such a dependence at later times $\tau > \tau_0$ either (this is the famous Bjorken result [114]). This reduces the originally (3+1)-dimensional equations (3.13) into (2+1) dimensions. The validity of this assumption is supported by the $dN/d\eta$-distributions measured at RHIC and LHC which are flat around midrapidity [35, 37, 60, 61].

[2] In addition, as mentioned in the previous Chapter, the elastic energy loss model described here explicitly decomposes the medium in terms of the Bose-Einstein and Fermi-Dirac distributions of free quarks and gluons.

[3] The momentum space rapidity is $y = \frac{1}{2}\log\frac{E+p_z}{E-p_z}$.

3.2.2 Equation of State

If the system has N different charges, the hydrodynamical equations (3.13) provide $4+N$ differential equations. However, there are $5+N$ independent variables: $\epsilon, p, v_x, v_y, v_z$ and N charge densities n_i. An additional equation is needed; this is the Equation of State which defines the relations between the local thermodynamical quantities ϵ, p and n_i and describes the transition from high-temperature quark-gluon plasma to low-temperature hadron resonance gas. This can be obtained from models such as the bag model [200], or extracted from lattice QCD calculations, like the s95x-series of equations of state [201].

3.2.3 Initial state

As the initial particle production in nucleus-nucleus collisions is a non-equilibrium process, it cannot be described by hydrodynamics. Thus the initial conditions for the hydrodynamical evolution must be obtained by other means.

The Glauber model can be used to estimate the number density of binary collisions n_{BC} or wounded nucleons n_{WN} in the transverse plane of the collision (which is all that is needed in the case of longitudinal boost-invariance). The initial energy density ϵ or entropy density s can then be assumed to be directly proportional to n_{BC} or n_{WN}. The transverse profiles obtained this way are known as ϵBC, ϵWN, sBC and sWN [202].

The above procedure leaves open the question of thermalization time τ_0. One way to fix τ_0 is using the EKRT minijet saturation model [203]. As a consequence of the uncertainty principle, a minijet (partonic jet with $p_T \lesssim 3-5$ GeV [204]) with transverse momentum p_T created in a nucleon-nucleon collision will occupy an area of the size $\sim \pi/p_T^2$. The saturation limit p_{sat} is reached when the number $N(p_{\mathrm{sat}})$ of produced minijets with $p_T > p_{\mathrm{sat}}$ is so large that (in a central collision) they fill the whole nuclear transverse area πR_A^2,

$$N(p_{\mathrm{sat}})\frac{\pi}{p_{\mathrm{sat}}^2} = \pi R_A^2. \tag{3.15}$$

After this point, any new gluons that form start fusing together with the ones already formed and the number of produced particles saturates. If the system is assumed to be also thermalized at the saturation time $\tau_{\mathrm{sat}} = 1/p_{\mathrm{sat}}$, the initial time is $\tau_0 = \tau_{\mathrm{sat}}$ for the hydrodynamical evolution. For the most central Au+Au collisions at RHIC with $\sqrt{s_{NN}} = 200$ GeV, $\tau_0 = 0.17$ fm, while for the central Pb+Pb collisions in the LHC with $\sqrt{s_{NN}} = 5.5$ TeV, the thermalization time is $\tau_0 = 0.1$ fm [205].

The EKRT model provides the initial time for the hydrodynamical evolution (and consequently, the energy loss simulation) in all studies of this thesis, except the static medium where the initial time is $\tau_0 = 0$.

3.2.4 Decoupling

As the system expands, it also becomes more dilute. Eventually the interactions between particles become so rare that thermal equilibrium cannot be maintained any longer and the hydrodynamical description breaks down again. Particles do not behave collectively any more; they *decouple* from the thermal part of the system. Decoupling implies that momentum distributions do not receive any further modifications, they *freeze out*. The problem with describing the decoupling is similar to that of initial conditions; hydrodynamics cannot be applied, different physics modeling must be used for the freeze-out process.

If the freeze-out is taken to be an instantaneous process, a sharp boundary is formed in space-time with the collective state on one side and free particles on the other side. This boundary, the decoupling surface, is determined by the freeze-out condition, which can be a certain value of temperature, for example. The particle emission from the decoupling surface can be then calculated with the Cooper-Frye formula [206]:

$$E\frac{dN_i}{d^3p} = \int_\sigma f_i(x,p)p^\mu d\sigma_\mu, \tag{3.16}$$

where the integral is over the decoupling surface σ and $f_i(x,p)$ is the Fermi-Dirac or Bose-Einstein distribution, depending on which type of particles i are being counted. This is the procedure utilized also in this thesis. Finally, the hydrodynamical models must consider also the decays of heavy resonance hadrons, but as these are not of direct relevance for the present work, they are omitted here.

3.3 Primary hard process

3.3.1 Factorization

In reality, we never see bare quarks or gluons, but their bound states, i.e. hadrons. This unfortunately means that the cross sections of the real scattering processes are not computable with perturbative QCD alone. This is where the concept of *factorization* comes in. Factorization theorems separate (factorize) the perturbatively calculable parts from the nonperturbative functions describing the distribution of partons in a hadron or, for the final state, hadrons produced from a parton [207]. The crucial feature of factorization theorems is that these distributions are *universal*; once they are defined for one process, the same functions should work for all the other processes as well. This makes it possible to make predictions for other measurements, a vital element of any physical theory.

Schematically, in vacuum, the factorized cross section for the inclusive production of a hadron h in an A+B collision can be expressed as

$$d\sigma^{AB\to h+X} = \sum_{ijk} f_{i/A}(x_1,Q^2)f_{j/B}(x_2,Q^2)\otimes d\hat{\sigma}^{ij\to k+x}(x_1,x_2,\alpha_s(\mu^2))\otimes D_{k\to h}(z,\mu_F^2),$$

where $f_{i/A}$ and $f_{j/B}$ are the *parton distribution functions* for the hadrons (or nuclei) A and B, respectively, and $\hat{\sigma}^{ij\to k+x}$ is the partonic cross section computable in pQCD, while $D_{k\to h}$ is the *fragmentation function* for forming the hadron h from the parton k. The renormalization scale is μ while Q and μ_F are the factorization and fragmentation scales, respectively.

3.3.2 Monte Carlo implementation

The factorization is a well-established concept only for the vacuum case. For the Monte Carlo model presented here, the use of factorization to generate the initial parton spectrum in nucleus-nucleus collisions is justified on the basis that the hard partons are formed before the formation of the medium.

The parton distributions for protons within a nucleus differ from those of free protons, $f_{a/p}(x,Q^2) \neq f_{a/A}(x,Q^2)$, and modifications are thus needed [212–217]. These nuclear modifications should be accounted for in the calculation of initial parton spectra for nucleus-nucleus collisions; they are ignored in this thesis, however, since for the p_T-range studied here these effects remain small ($\lesssim 10\%$).

Based on the factorization, the LO pQCD production spectrum for the parton i in nucleus-nucleus collisions – which here means proton-proton collisions, as for simplicity the nucleus is assumed to consist only of protons – is (see, e.g. Ref. [208])

$$\begin{aligned}\frac{d\sigma^{pp\to i+X}}{dp_T^2 dy_i} &= \int dy_1 dy_2 \sum_{(kl)} \frac{d\sigma^{pp\to kl+X}}{dp_T^2 dy_1 dy_2} \\ &\cdot \left[\delta_{ki}\delta(y_i - y_1) + \delta_{li}\delta(y_i - y_2)\right] \frac{1}{1+\delta_{kl}},\end{aligned} \tag{3.17}$$

where

$$\frac{d\sigma^{\,pp\to kl+X}}{dp_T^2 dy_1 dy_2} = \sum_{ab} x_1 f_a(x_1,Q^2) x_2 f_b(x_2,Q^2) \frac{d\hat{\sigma}^{ij\to kl}}{d\hat{t}} \tag{3.18}$$

with $d\hat{\sigma}/d\hat{t}$ containing the squared, spin- and color-summed/averaged leading-order pQCD matrix elements for $2 \to 2$ -processes (see e.g. Ref. [209] or Appendix A of Paper [I]). This spectrum, calculated at midrapidity $y_i = 0$ and for transverse momentum $p_{T\min} \leq p_T \leq \sqrt{s}/2$, is used to generate the initial distribution of hard partons for the Monte Carlo simulation. For the parton distribution functions, the set CTEQ6L1 [210, 211] is used.

The flavor i of the initial hard parton is determined from the probabilities given by (3.17) integrated from p_{Tmin} to some limit value $p_{Tmin} \ll p_{Tlimit} \leq \sqrt{s}/2$, normalized by the flavor-summed total cross section. The method is very simple: Arrange the probabilities $\mathcal{P}_i$ of the different flavors i on a line segment of length 1: Flavor 1 corresponds to interval $[0, \mathcal{P}_1]$ on the line, flavor 2 to $[\mathcal{P}_1, \mathcal{P}_1 + \mathcal{P}_2]$, flavor 3 to $[\mathcal{P}_1 + \mathcal{P}_2, \mathcal{P}_1 + \mathcal{P}_2 + \mathcal{P}_3]$ etc. Pick a uniform random number R between $[0, 1]$. The flavor of the hard parton is the one corresponding to the interval containing R.

The sampling of initial transverse momentum p_{Ti} of the hard parton also has probabilities on a line segment, but uses additionally the inverse integral function of the probability density function. Here the integral $I_i(p_T)$ of (3.17) over an interval $p_{Tmin} \leq p_T \leq p_{Tmax}$ is tabulated for each flavor i, with p_{Tmax} increasing in 1 GeV steps up to the limit value $p_{Tlimit} \leq \sqrt{s}/2$. The corresponding p_T in each momentum bin is taken to be $p_{Tmax} - 0.5$. A random number R is selected between 0 and $I_i(p_{Tlimit})$. The first tabulated p_T value for which $I_i(p_T) \leq R$ is chosen as p_{Ti}.

3.4 2-to-2 scattering in leading order pQCD

3.4.1 Scattering rate

A parton i with (high) energy E_1 traversing strongly interacting medium in a temperature T, will interact with the thermal particles j which have momentum distribution $f_j(p_2 \cdot u, T)$. The scattering rate for a process $ij \to kl$ is (see, for example, Ref. [105, 218])

$$\begin{aligned}\Gamma_{ij\to kl} =& \frac{1}{2E_1}\int\frac{d^3p_2}{(2\pi)^3 2E_2}\int\frac{d^3p_3}{(2\pi)^3 2E_3}\int\frac{d^3p_4}{(2\pi)^3 2E_4} \\ & f_j(p_2\cdot u, T)\,|M|^2_{ij\to kl}(s,t,u)\,S_2(s,t,u) \\ & (2\pi)^4\delta^{(4)}(p_1+p_2-p_3-p_4),\end{aligned} \tag{3.19}$$

where the 4-momenta are p_1 for the hard parton i, p_2 for the thermal particle j and p_3, p_4 for the final state particles k and l.

In general, the scattering rate depends on the frame, and in particular on the high-energy parton's 4-momentum p_1, on the flow 4-velocity $u(x)$ and on the temperature $T(x)$ of the fluid at each space-time location x.

The distribution function for a thermal particle of momentum p_2 is denoted by $f_j(p_2 \cdot u, T)$, which is the Bose-Einstein distribution $f_{BE} = g_g(1+e^{-p_2\cdot u/T})^{-1}$ for gluons and the Fermi-Dirac distribution $f_{FD} = g_q(1-e^{-p_2\cdot u/T})^{-1}$ for quarks. To be exact, one should also include the Bose enhancement and Pauli blocking factors $(1 \pm f(p,T))$ for the final state thermal particle, but as these are small corrections compared to other uncertainties of the model, they are ignored in this study.

The initial state spins and colors have been averaged over in the squared matrix elements $|M(s,t,u)|^2$, represented as a function of the Mandelstam variables $s = (p_1+p_2)^2$, $t = (p_1-p_3)^2$ and $u = (p_1-p_4)^2$. Thus, the spin- and color-degeneracy factors in f_{BE} and f_{FD} are $g_g = 2\cdot 8 = 16$ for gluons, and $g_q = 2\cdot 3 = 6$ for quarks and antiquarks. Additional factors stem from acceptable quark flavors in a process, for example if $i = u$ in the $q_iq_j \to q_iq_j$ -scattering (where $i \neq j$), j can be $d, s, \bar{d}$ or $\bar{s}$, thus giving an additional factor 4. In the simulations of this thesis, the scattering rate is always calculated in the local

rest-frame of the fluid (like in MARTINI), so that $p_2 \cdot u = E_2$ and E_1 is the energy of the high-energy parton i in this frame.

The scattering amplitudes have singularities at $t, u \to 0$ and thus must be regularized. In this thesis a cut-off scale $m = s_m g_s T$, inspired by the Debye screening mass mentioned in Chapter 2, is introduced so that $u, t \leq -m^2$. Here s_m is a free parameter of the model, typically kept close to unity. The strong coupling g_s is kept constant in all simulations presented in this thesis. Since for massless particles $s + u + t = 0$, the cut-off conditions are equivalent to $-s + m^2 \leq t \leq -m^2$ with the requirement $s \geq 2m^2$. These conditions are encoded in the function S_2, which is defined as

$$S_2(s, t, u) = \theta(s \geq 2m^2)\theta(-s + m^2 \leq t \leq -m^2). \tag{3.20}$$

Strictly speaking, the most complete analogy with thermal mass is achieved when the regulator is introduced in the scattering amplitudes instead of integral limits. The difference of the two regularization schemes has been investigated in JEWEL [89]; using the regulator in the integral limits was found to increase the energy loss by roughly a factor 2 compared to the regulator in the amplitudes. However, as increasing m in the integral limits has two opposite effects on the energy loss – the decrease of the scattering rate and the increase of the minimum allowed momentum transfer in a scattering event – it is not obvious how the difference between the two schemes behaves as a function of m. While the difference is good to keep in mind when comparing different energy loss models, the parameters α_s and s_m do provide a good control over the magnitude of the energy loss within the model under study here. The issue is thus left for a future investigation.

In terms of the scattering cross section

$$\begin{aligned}\sigma_{ij\to kl}(s) =& \frac{1}{1+\delta_{kl}} \frac{1}{2s} \int \frac{d^3p_3}{(2\pi)^3 2E_3} \int \frac{d^3p_4}{(2\pi)^3 2E_4} S_2(s,t,u) \\ & \cdot (2\pi)^4 \delta^{(4)}(p_1 + p_2 - p_3 - p_4) \, |M|^2_{ij\to kl}(s,t,u), \\ =& \frac{1}{1+\delta_{kl}} \frac{1}{16\pi s^2} \int_{-s+m^2}^{-m^2} dt \, |M|^2_{ij\to kl} \theta(s \geq 2m^2),\end{aligned} \tag{3.21}$$

where δ_{kl} takes care of the phase space double counting in the case of identical final state particles, Eq. (3.19) can be expressed as

$$\Gamma_{ij\to kl} = \int \frac{d^3p_2}{(2\pi)^3} f_j(E_2, T) \theta(s \geq 2m^2) \frac{2s}{2E_1 2E_2} \sigma_{ij\to kl}(s), \tag{3.22}$$

Manipulating $s = 2E_1E_2(1 - \cos\theta_{12})$ into an integration variable, one gets

$$\Gamma_{ij\to kl} = \frac{1}{16\pi^2 E_1^2} \int_{\frac{m^2}{2E_1}}^{\infty} dE_2 f_j(E_2) \Omega_{ij\to kl}(E_1, E_2, m^2), \tag{3.23}$$

where

$$\Omega_{ij\to kl}(E_1, E_2, m^2) = \int_{2m^2}^{4E_1E_2} ds[s\sigma_{ij\to kl}(s)]. \tag{3.24}$$

Inserting the expression (3.21) for the cross section into the definition of the Ω-function (3.24) gives

$$\begin{aligned}&\Omega_{ij\to kl}(E_1, E_2, m^2)\\ &\quad= \frac{1}{1+\delta_{kl}}\frac{1}{16\pi}\int_{2m^2}^{4E_1E_2} ds\left[\frac{1}{s}\int_{-s+m^2}^{-m^2} dt|M|^2_{ij\to kl}\right].\end{aligned} \tag{3.25}$$

Certain terms appear generically in several amplitudes. It is thus simpler to list the integrals for each of these terms separately, and the appropriate terms can then be combined to form the final expressions for $\Omega_{ij\to kl}(E_1, E_2, m^2)$. All these terms are listed in Appendix A of Paper [I].

The total scattering rate for a high-energy parton of a type i is then a sum of all the possible channels,

$$\Gamma_i(p_1, u(x), T(x)) = \sum_{j(kl)} \Gamma_{ij\to kl}(p_1, u(x), T(x)), \tag{3.26}$$

where the possible processes $ij \to kl$ are accounted for by summing over all types of collision partners, $j = g, u, d, s, \bar{u}, \bar{d}, \bar{s}$ in the initial state, and all possible parton type pairs (kl) in the final state. The obtained scattering rates Γ_i for quarks, antiquarks and gluons, along with the contributions $\Gamma_{ij\to kl}$ from different processes, are shown in Fig. 3.2 as a function of temperature T and in Fig. 3.3 as a function of the hard parton energy E_1.

Considering the process $ij \to kl$, the average of the quantity A in a medium at temperature T can be computed in the rest frame of the fluid as

$$\begin{aligned}\langle A\rangle_{ij\to kl} \equiv &\frac{1}{\Gamma_{ij\to kl}}\int \frac{d^3p_2}{(2\pi)^3} f_j(E_2, T)\cdot A\cdot\\ &\theta(s \geq 2m^2)(1-\cos\theta_{12})\sigma_{ij\to kl}(s).\end{aligned} \tag{3.27}$$

At the high-energy limit, $E_1^2, s \gg m^2, T^2$, the relevant pQCD cross sections all behave as $\sigma \sim m^{-2}$, and $\sigma_{gg\to gg} \approx \frac{9}{4}\sigma_{gq\to gq} \approx (\frac{9}{4})^2\sigma_{q_iq_j\to q_iq_j}$. Using the Boltzmann distribution for the thermal particles, the following averages for the quantities relevant in a scattering process can be computed [I]:

$$\langle s\rangle \approx 8E_1T, \qquad \langle E_2\rangle \approx 3T, \qquad \langle\cos\theta_{12}\rangle \approx -\frac{1}{3}. \tag{3.28}$$

Furthermore, analytical estimates for the scattering rates can be produced [I]:

$$\begin{aligned}
\Gamma_g &\approx \Gamma_{gg\to gg} + \sum_i [\Gamma_{gq_i\to gq_i} + \Gamma_{g\bar{q}_i\to g\bar{q}_i}] \\
&\approx (g_g + 2\cdot 3\cdot g_q\cdot \tfrac{4}{9})\frac{9}{2}\frac{\alpha_s^2 T^3}{\pi m^2} = 144\frac{\alpha_s^2 T^3}{\pi m^2} = 36\frac{\alpha_s T}{\pi^2 s_m^2}, \qquad (3.29) \\
\Gamma_{q_i} &\approx \Gamma_{q_i g\to q_i g} + \sum_j [\Gamma_{q_i q_j\to q_i q_j} + \Gamma_{q_i\bar{q}_j\to q_i\bar{q}_j}] \\
&\approx (g_g\cdot \tfrac{4}{9} + 2\cdot 3\cdot g_q\cdot (\tfrac{4}{9})^2)\frac{9}{2}\frac{\alpha_s^2 T^3}{\pi m^2} = 64\frac{\alpha_s^2 T^3}{\pi m^2} = 16\frac{\alpha_s T}{\pi^2 s_m^2}, \qquad (3.30)
\end{aligned}$$

where the factors $2\cdot 3$ account for quarks and antiquarks times the number of quark flavors.

These estimates are shown together with the actual scattering rates in Figs. 3.2 and Fig. 3.3. The agreement with the exact calculation and the above crude estimate is surprisingly good.

3.4.2 Scattering probability

In the Monte Carlo simulation under study here, the scattering rates are used to determine when the hard partons interact with the medium. Taking a time interval Δt, the average number of collisions expected in this interval is $\langle n_c\rangle = \Gamma_i \Delta t$. According to the Poisson distribution, the probability for n_c collisions in Δt is then

$$P(n_c \text{ collisions in } \Delta t) = e^{-\Gamma_i \Delta t}\frac{(\Gamma_i \Delta t)^{n_c}}{n_c!}, \qquad (3.31)$$

and in particular the probability for no collisions in the time interval Δt is

$$P(\text{No collisions in } \Delta t) = e^{-\Gamma_i \Delta t}. \qquad (3.32)$$

As mentioned above, the scattering rate Γ_i is calculated in the local rest frame of the fluid. Because of this, the time step Δt must be boosted into the same frame: $\Delta t \to \Delta t' = \frac{\Delta t}{\gamma}$, where $\gamma = \frac{1}{\sqrt{1-|\mathbf{v}|^2}}$ is the Lorentz factor while $\mathbf{v}$ is the fluid 3-velocity. And since Γ_i also depends on temperature, which in general does not remain constant in time, the probability must be recalculated at every step.

The scattering process $ij \to kl$ which happens in a scattering event is determined by the probabilities given by the ratio to total scattering rate Γ_i.

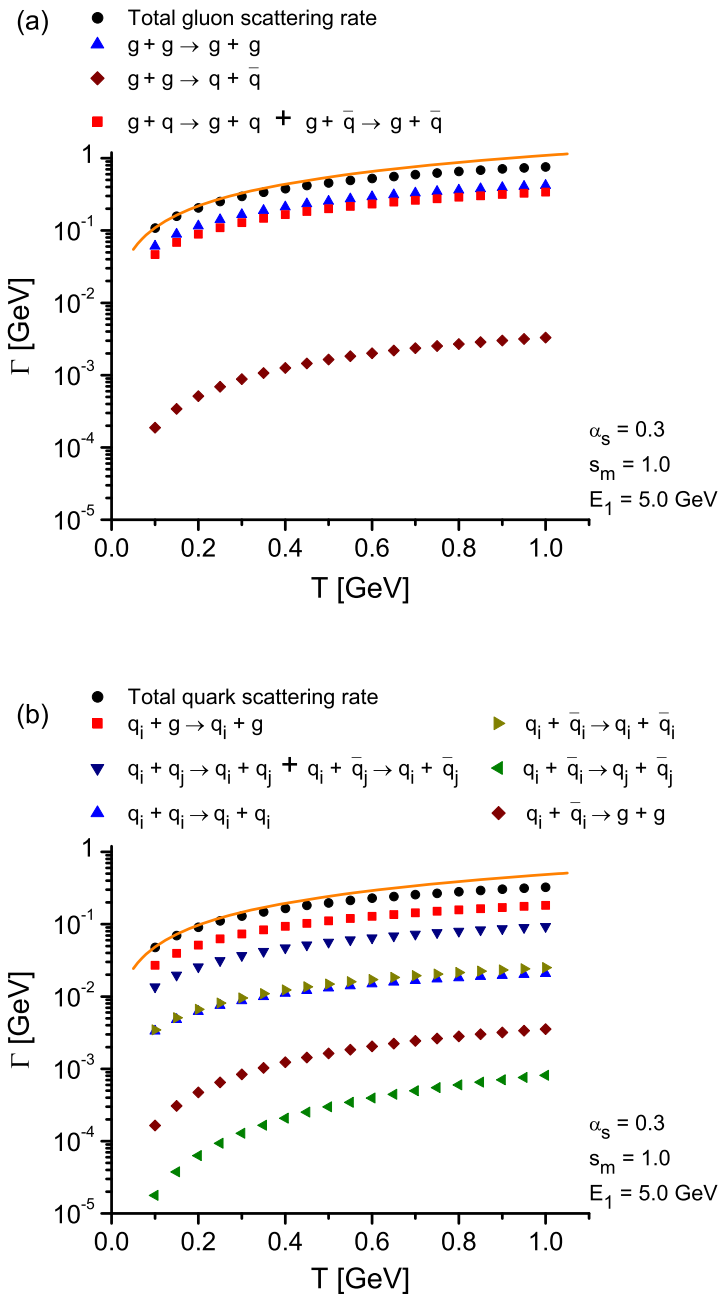

Figure 3.2: The scattering rates Γ_i of gluon (above) and quark (below) as a function of temperature T for a QCD plasma at rest. Flavor- and quark-antiquark -summed contributions from different processes and the analytical estimates for the total rates discussed in the text are also shown (solid lines). From Paper [I].

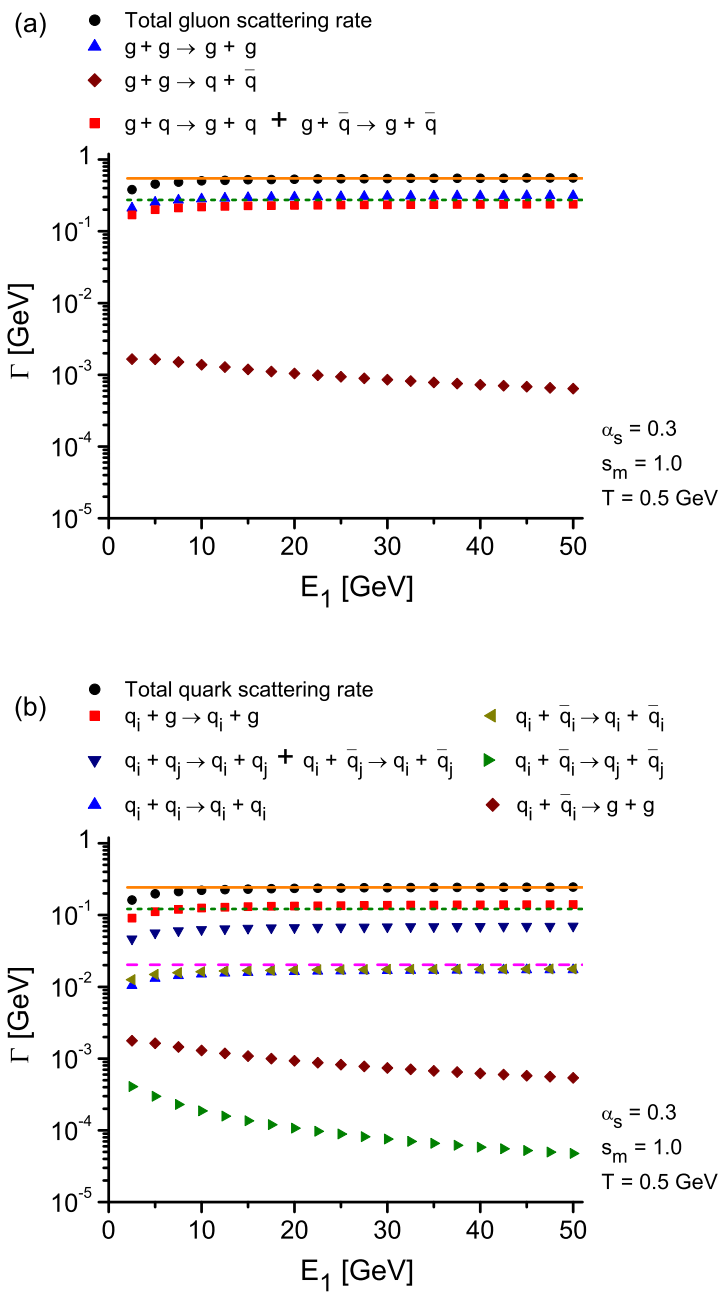

Figure 3.3: The scattering rates Γ_i of gluon (above) and quark (below) as a function of the parton energy E_1, for a QCD plasma at rest at $T = 0.5$ GeV. Flavor-summed contributions from different processes are shown. The analytical estimates for Γ_i (see text) are shown by the solid lines. In the upper panel, the analytical estimate for the $gg \to gg$ process (dashed line) is the same as for the quark-antiquark summed $gq \to gq$ process. In the lower panel, the dashed lines show the contributions from the $q_i g \to q_i g$ process and an individual $q_i q_j \to q_i q_j$ process. From Paper [I].

3.4.3 Execution of scattering event

Typically, it is most practical to calculate the hard-parton+medium-parton scattering processes in the center-of-mass (CMS) frame of the two scatterers. At the beginning of a scattering calculation, the scattering particles are in the local rest frame of the fluid where they have four-momenta $p_1 = (E_1, \mathbf{p}_1)$ and $p_2 = (E_2, \mathbf{p}_2)$. The energy E_2 of the medium particle is sampled from the integrand of the scattering rate (3.23) using the hit-or-miss method (which was used earlier to select the initial transverse position of the hard parton). The inverse integral function method is used for sampling the collision angle $\cos\theta_{12}$ from the $s\sigma_{ij\to kl}(s)$ function after E_2 is determined, using the relation $s = 2E_1E_2(1-\cos\theta_{12})$. In essence, the function $I_\Omega(s)$ is defined as an indefinite integral version of the Ω function (3.24). $I_\Omega(s)$ does not have an analytical inverse function, but s is numerically solved from the equation $I_\Omega(s) - R = 0$, where R is a random number between $I_\Omega(s_{\min})$ and $I_\Omega(s_{\max})$.

In the local rest frame of the fluid, the CMS of the scatterers has the 3-velocity $\mathbf{v}_{\rm CMS} = \frac{\mathbf{p}_1+\mathbf{p}_2}{E_1+E_2}$. The Lorentz boost gives the energies and momenta of the two particles in CMS frame:

$$\begin{aligned} E' &= \gamma(E - \mathbf{v}_{\rm CMS}\cdot\mathbf{p}), \\ \mathbf{p}' &= \mathbf{p} + \gamma\mathbf{v}_{\rm CMS}(\frac{\gamma}{\gamma+1}\mathbf{p}\cdot\mathbf{v}_{\rm CMS} - E), \end{aligned} \tag{3.33}$$

where γ is the Lorentz factor $\frac{1}{\sqrt{1-\mathbf{v}_{\rm CMS}{}^2}}$. In these coordinates $\mathbf{p}_2' = -\mathbf{p}_1'$ and $E_1' = E_2' = \sqrt{s}/2$. However, the orientation of the 3-momentum vectors with respect to the coordinate axes is arbitrary: Expressed in spherical coordinates, $p_1' = E_1'(1, \sin\psi\cos\phi, \sin\psi\sin\phi, \cos\psi)$ with the zenith angle ψ and azimuth angle ϕ. To complete the transformation, the system is rotated so that the 3-momentum part of $(p_1^*)^\mu = R^{\mu\nu}(p_1')_\nu$ lies on the z-axis. The required rotation matrix R is

$$R = \begin{pmatrix} 1 & 0 & 0 & 0 \\ 0 & \cos\psi\cos\phi & \cos\psi\sin\phi & -\sin\psi \\ 0 & -\sin\phi & \cos\phi & 0 \\ 0 & \sin\psi\cos\phi & \sin\psi\sin\phi & \cos\psi \end{pmatrix}. \tag{3.34}$$

The inverse function method is used for sampling the scattering angle $\cos\theta_{13}^* = \frac{2t}{s} + 1$ from the indefinite integral $\sigma(t) = \int dt \frac{d\sigma}{dt}$. Again, the inverse of $\sigma(t)$ does not have an analytical form, but the desired variable t is solved from the equation $\sigma(t) - R = 0$, $R \in [\sigma(t_{\min}), \sigma(t_{\max})]$.

When the post-scattering 4-momenta p_3^*, p_4^* have been computed, the return to initial coordinate frame is done with an inverse rotation

$$R^{-1} = \begin{pmatrix} 1 & 0 & 0 & 0 \\ 0 & \cos\psi\cos\phi & -\sin\phi & \sin\psi\cos\phi \\ 0 & \cos\psi\sin\phi & \cos\phi & \sin\psi\sin\phi \\ 0 & -\sin\psi & 0 & \cos\psi \end{pmatrix} \tag{3.35}$$

and inverse boost

$$\begin{aligned} E &= \gamma(E' + \mathbf{v}_{\mathrm{CMS}} \cdot \mathbf{p}'), \\ \mathbf{p} &= \mathbf{p}' + \gamma \mathbf{v}_{\mathrm{CMS}}(\frac{\gamma}{\gamma+1}\mathbf{p}' \cdot \mathbf{v}_{\mathrm{CMS}} + E'). \end{aligned} \tag{3.36}$$

Finally, both four-momenta must yet be boosted from the local rest frame of the plasma to the laboratory frame in order to decide which one is the highest-energy parton to be followed at the next time step.

3.5 Hadronization

The end result of the Monte Carlo simulation described here is the medium-modified distribution of high-energy leading partons, $\frac{dN^{AA\to f+X}}{dp_T dy}$. In order to compare with experimental observables, this distribution must be hadronized. This is done in the spirit of the factorization described in Section 3.3.1, by convoluting the obtained partonic distribution with the fragmentation function $D_{f\to\pi}(z, \mu_F^2)$:

$$\begin{aligned} \frac{dN^{AA\to h+X}}{dP_T dy} = \sum_f \int dp_T dy \frac{dN^{AA\to f+X}}{dp_T dy} \cdot \\ \int_0^1 dz D_{f\to h}(z, \mu_F^2) \delta(P_T - z p_T), \end{aligned} \tag{3.37}$$

where $z = \frac{P_T}{p_T}$ is the fraction of the final parton momentum p_T available to the hadron with momentum P_T, and $\mu_F \sim P_T$ is the fragmentation scale. The fragmentation functions used in this thesis are those of Kniehl, Kramer and Pötter [219].

Chapter 4

Results

In this Chapter, the Monte Carlo simulation described in the previous Chapter is used for investigating the elastic energy loss of hard partons in several different scenarios. The results for the static medium are analyzed first, as this allows for comparisons against the other similar models. The focus then moves to the actual heavy ion collisions and comparisons against the experimental data, using more and more sophisticated hydrodynamical backgrounds as the investigated observables become more involved.

4.1 Static medium

The static, uniform medium – in other words, a constant-temperature medium without flow – is not a realistic description of the quark-gluon plasma. However, it does offer a suitable setting for testing the properties of energy loss models and makes it easier to compare different models against each other. One such setting for the model comparisons is the Brick problem (static, uniform medium with a fixed length), which has been generally agreed by the modeling community to be the testing scenario for the different energy loss models [220].

When moving from RHIC to the LHC, one arising feature is the stronger P_T dependence of the nuclear modification factor $R_{AA}(P_T)$. This is due to the less steeply falling P_T spectrum of the produced particles in the LHC, which allows for probing the energy loss probability distribution $P(\Delta E)$ over a wider range of energy loss ΔE. The convolution of $P(\Delta E)$ with the P_T spectrum dN/dP_T corresponds to a suppression of partons, since the parton with final energy E must originate from some higher energy $E + \Delta E$, which – due to the falling P_T spectrum – has fewer partons to begin with. At RHIC, dN/dP_T drops so fast and the high-P_T range with experimental data is so small that only a small portion of $P(\Delta E)$ can be probed [221, 222].

Several collisional energy loss models use the diffusion approximation (for example [153, 157, 161]). In such a scenario the energy loss probability distribution is a Gaussian and the average value of energy loss provides a good estimate for the overall energy loss. The Gaussian parametrization gives a rather good

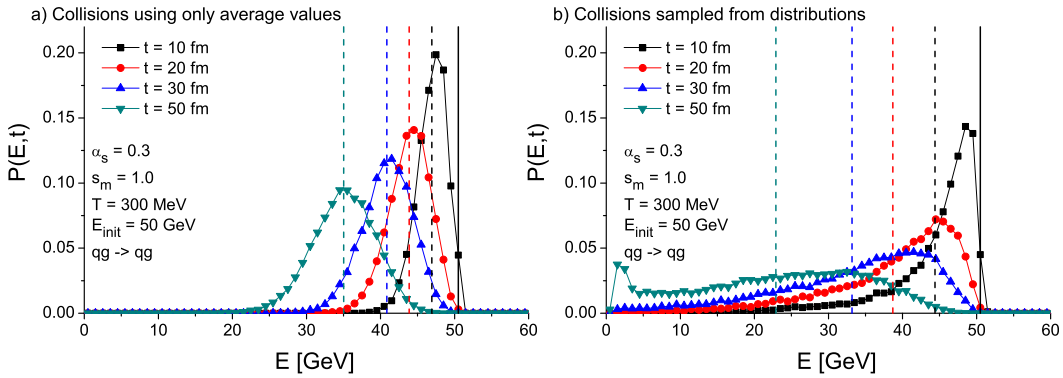

Figure 4.1: a) The probability distribution for the energy of a 50 GeV quark after traveling in gluon plasma for various time periods, using average values for the scattering variables $\hat{t}, E_2$ and $\cos\theta_{12}$. b) As a), but the scattering variables are sampled from their respective distributions. Dashed vertical lines illustrate the average energy values, while the solid line marks the initial energy bin. The temperature of the medium is $T = 300$ MeV, the value of the strong coupling is $\alpha_s = 0.3$ and the regulator mass parameter is $s_m = 1.0$. From Paper [V].

agreement with the $R_{AA}(P_T)$ of the LHC [180], as the majority of the particles suffer roughly the same amount of energy loss.

To study the validity of such an assumption, in Paper [V] the momentum exchange between the hard parton and the medium particle was treated in two different ways. The "correct" way is to sample the Mandelstam-$\hat{t}$ from the distribution $\frac{d\sigma}{d\hat{t}}^{ij\to kl}$. The other method mimics the diffusion approximation and uses the average Mandelstam-$\hat{t}$,

$$\langle \hat{t} \rangle = \frac{\int_{-\hat{s}+m^2}^{-m^2} d\hat{t}\, \hat{t} \frac{d\sigma}{d\hat{t}}}{\int_{-\hat{s}+m^2}^{-m^2} d\hat{t} \frac{d\sigma}{d\hat{t}}}. \tag{4.1}$$

In this method, all scatterings are done with the average momentum exchange. In addition, the average values calculated in Chapter 3 are used also for the energy of a thermal parton $\langle E_2 \rangle = 3T$ and the collision angle $\langle \cos\theta_{12} \rangle \approx -\frac{1}{3}$. Furthermore, the amplitude of the process $qg \to qg$ has been approximated with a pure $\hat{t}$-channel: $|M|^2_{qg\to qg} \propto \frac{\hat{s}^2+\hat{u}^2}{\hat{t}^2}$.

Figure 4.1 shows the difference between the two scenarios described above for an initial 50 GeV quark traveling in the purely gluonic medium for several different periods of time. As expected, using the average values for each scattering event produces Gaussian distributions. However, when the scattering variables are actually sampled from their respective distributions, the form of the energy probability distribution is quite different – reminiscent of the distribution produced by the radiative energy loss, in fact [142]. The fact that both MARTINI and BAMPS – the two energy loss models which treat the elastic energy loss

in a way similar to the one used here – produce qualitatively[1] similar distributions [142, 189] provides assurance that the dynamics of the elastic energy loss are correctly realized in the simulations done in this thesis.

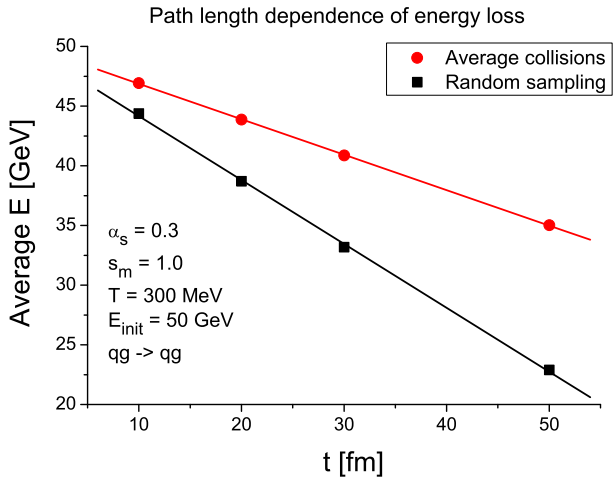

Figure 4.2: Comparison of the hard parton average energy pathlength dependence in average collisions scheme and the distribution sampling scheme. Solid circles correspond with the dashed lines shown in Fig. 4.1 a) and solid squares correspond with the dashed lines shown in Fig. 4.1 b). The temperature of the medium is $T = 300$ MeV, the strong coupling constant value is $\alpha_s = 0.3$ and the regulator parameter $s_m = 1.0$. From Paper [V].

Clearly in the "correct" scenario the average values (dashed lines) provide a less meaningful description of the magnitude of the energy loss, as the variation around the mean is large and strongly asymmetric. Nevertheless, as seen in Fig. 4.2, the dependence of the average energy loss on the in-medium pathlength L remains linear in both cases. Thus the assumptions about the shape of $P(\Delta E)$ do not seem to play a role in the studies of pathlength-dependent features of the energy loss.

4.2 Central collisions at RHIC

The simplest realistic cases of relativistic heavy ion collisions that can be examined are the most central collisions, where the impact parameter $\mathbf{b} \approx 0$. Here the medium possesses an approximate azimuthal symmetry which simplifies the hydrodynamical modeling. This situation was investigated in Paper [I] for $\sqrt{s_{NN}} = 200$ GeV Au+Au collisions.

As discussed in [I], the medium in the beginning is assumed to be a collective state of massless quarks and gluons governed by (1+1)-dimensional hy-

[1] As the regularization schemes vary between models, quantitative differences are to be expected.

drodynamical equations [205] and the bag model equation of state, with initial conditions obtained from the EKRT model. As the system cools down to a critical temperature $T_C = 165$ MeV, it enters a mixed phase, gradually turning into a hadron gas. As temperature stays constant in the mixed phase while energy density ϵ keeps decreasing, an effective temperature

$$T_{eff} = (\frac{30}{g_Q \pi^2}(\epsilon - B))^{1/4}, \tag{4.2}$$

is used for scattering calculations in this model. Here $g_Q = g_g + \frac{7}{8} 2 N_f g_q = \frac{95}{2}$ is the quark-gluon plasma degrees of freedom and B is the bag constant. The interactions between the hard parton and hadron gas are assumed to be negligible (due to the substantially lower energy density and temperature of the hadron gas) and thus the Monte Carlo simulation ends after the mixed phase (i.e. when the actual temperature falls below T_C).

Since the focus here is on high-energy hadrons, only those partons with transverse momentum higher than $p_{T\min} \geq 5.0$ GeV are taken into account in the final results. During the simulation, partons which fall below $E = 3T$ are assumed to be thermalized and are dropped from the simulation. All observables are averaged across the rapidity window $[-0.35, 0.35]$ which corresponds to the acceptance of the PHENIX detector [147]. The initial rapidity window is chosen to be slightly larger, $y_{min} = -y_{max} = -1$, to make sure all partons which potentially could reach the final rapidity window will be accounted for.

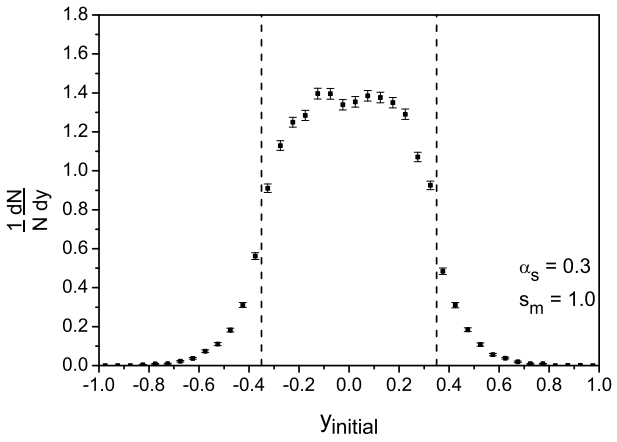

Figure 4.3: The initial rapidity distribution of the partons contributing to the final results. The final interval $|y| \leq 0.35$ is shown by the dashed lines. From Paper [I].

Fig. 4.3 demonstrates the contribution of particles at different initial rapidities to the final rapidity window in the default set-up with the strong coupling $\alpha_s = 0.3$ and thermal mass parameter $s_m = 1.0$. The amount of particles originated outside of the final rapidity interval is not very large, slightly over 10%.

This supports the notion that the often employed eikonal approximation – where hard partons travel on straight lines, and thus would keep their original rapidity – is an acceptable first approximation.

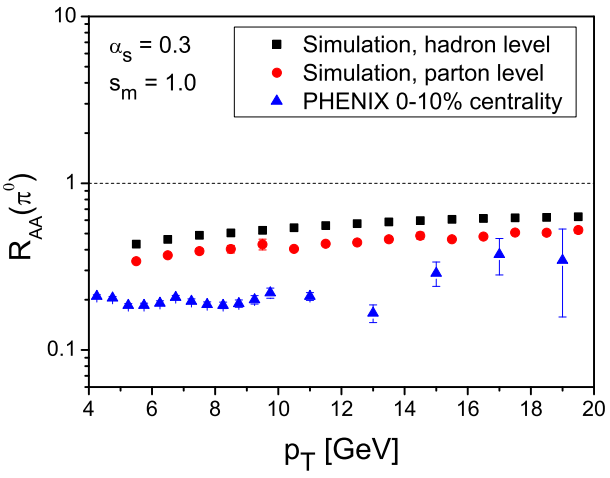

Figure 4.4: The nuclear modification factor, both for π^0 and partons, with strong coupling constant $\alpha_s = 0.3$ and mass parameter $s_m = 1.0$, compared with the PHENIX data from [147]. From Paper [I].

Figure 4.4 shows the nuclear modification factor R_{AA} both on the hadronic level and the partonic level, comparing it with the π^0 data from PHENIX [147]. With the "default" parameter values $\alpha_s = 0.3$, $s_m = 1.0$, the suppression from the elastic collisions alone is not enough to describe the data, but the suppression is nevertheless considerable.

Additionally, since $R_{AA}(p_T)$ is nearly flat[2], the convolution of the medium-modified parton spectrum with the fragmentation function does not alter the nuclear modification significantly. Thus it can be argued that for studying the qualitative behavior of the R_{AA}, the partonic level is sufficient. This is why many of the later Figures show only partonic R_{AA}, as it requires much less statistics to produce compared to hadronic R_{AA}, which requires integration over a steeply falling p_T spectrum. Indeed, to keep the statistical fluctuations reasonable, the simulation has to be done in several parts, each covering a p_T interval of ~ 5 GeV. For a reasonable good estimate of the hadronic spectrum from $P_T = 5$ GeV to 10 GeV, the partonic spectrum must reach from $p_T = 5$ GeV to at least 20 GeV, meaning three separate simulation runs with 5 GeV intervals.

Figure 4.5 demonstrates the effect of the mixed phase on the partonic nuclear modification factor. The effect is found to be small, which means that most of the suppression happens in the quark-gluon plasma phase. This gives *a posteriori*

[2]As discussed in the previous section, the RHIC experiments are insensitive to the shape of $P(\Delta E)$.

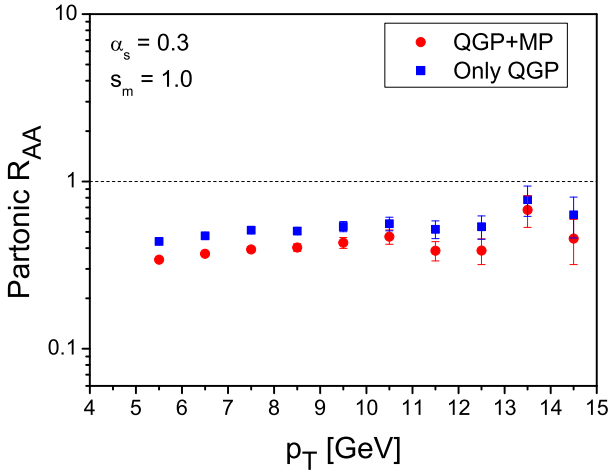

Figure 4.5: The parton-level nuclear modification factors with $\alpha_s = 0.3$ and $s_m = 1.0$, including only the scatterings in the QGP phase (squares) and in the QGP + mixed phase (circles). From Paper [I].

justification for ignoring the hadron gas phase (where energy density is even lower) in the study of central collisions and also in the following investigations of more complex systems.

The left panel of Figure 4.6 demonstrates the dependence of the partonic nuclear modification on the strong coupling α_s. As could be expected on the basis of the approximate analytic forms (3.29) and (3.30) of the scattering rate, changing α_s has a strong effect on the nuclear modification. Doubling the coupling approximately doubles the suppression in the examined range of α_s. With $\alpha_s = 0.6$, which is still an acceptable value for α_s in pQCD, the elastic contribution to the energy loss already takes the R_{AA} below the RHIC data.

To map out the systematic uncertainties of the model, the cutoff mass parameter s_m can be varied in the same way as α_s. The effect of this is presented in the right panel of Fig. 4.6. One would suppose that while the cross section increases when the cutoff limit is reduced, this increase in scattering rate is compensated by the lesser energy loss in a single collision due to the tendency towards smaller momentum transfers. However, for the examined values of s_m, the suppression keeps increasing with decreasing mass. One could argue some saturation happening at $p_T > 11$ GeV; however, here the statistical fluctuations start to be notable, obscuring the interpretation. Apparently the forward scattering, which would be inefficient for the energy loss, requires a very small regulator, $s_m < 0.25$.

Figure 4.7 can be considered as a "tomography" image, showing the distribution of initial positions of the partons which survived out of the medium for three different values of strong coupling constant. The position of each particle is rotated in the transverse xy-plane so that they all move to the direction of

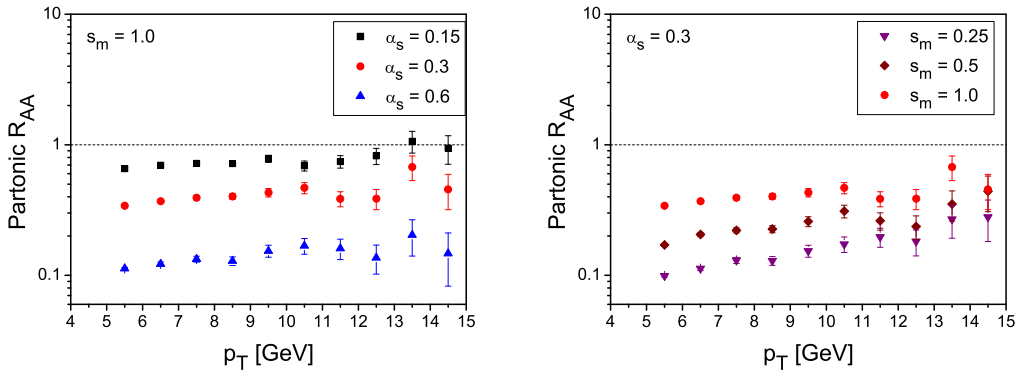

Figure 4.6: Left panel: Parton level nuclear modification factor R_{AA} for the regulator-mass parameter value $s_m = 1.0$ and strong coupling constant values $\alpha_s = 0.15, 0.3, 0.6$. Right panel: Parton level R_{AA} for mass parameter values $s_m = 0.25, 0.5, 1.0$ and strong coupling constant $\alpha_s = 0.3$. From Paper [I].

positive x-axis. For $\alpha_s = 0.15$ (upper panel), the most dense area of the distribution has moved only slightly from the origin, implying that the medium is almost transparent at this value of the coupling. When the value of α_s is doubled to 0.3 (middle panel), the peak of the distribution clearly moves off from the center. The partons from the center do not survive through the medium any longer and thus a bias towards surface areas appears. The effect is emphasized when the coupling is doubled a second time (bottom panel). This implies that when α_s is large, the partons contributing to the final results come from the surface region and very little information from the hot center can be obtained from the available observables.

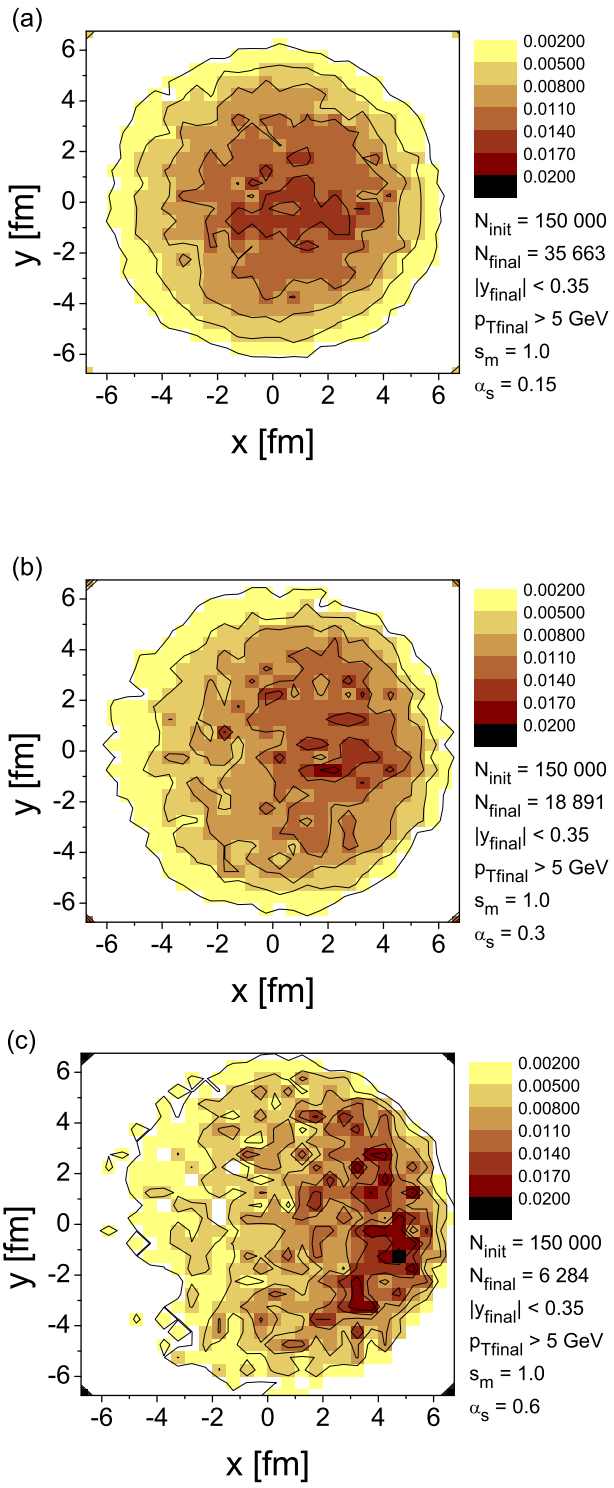

Figure 4.7: Initial production points of the partons contributing to the final results on the transverse plane for $\alpha_s = 0.15$ (above) $\alpha_s = 0.3$ (middle)and $\alpha_s = 0.6$ (below). All particles are moving to the positive x-direction. From Paper [I].

4.3 Non-central collisions at RHIC

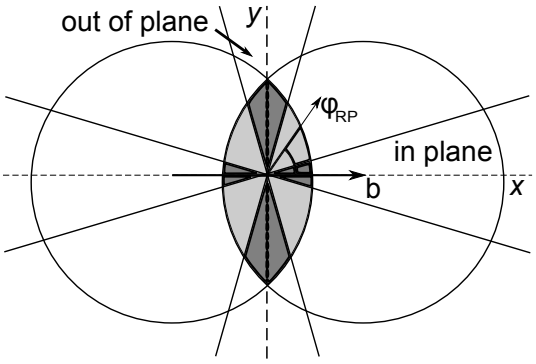

Figure 4.8: A sketch of the reaction plane dependence of the nuclear modification. The in-plane direction is parallel to the impact parameter **b**, while the out-of-plane direction is perpendicular to it. The dark gray areas illustrate the in-plane and out-of-plane binning.

Non-central nuclear collisions have a somewhat more complicated geometry compared to the central collisions. The azimuthal anisotropy of the collision event means that for a particle starting from the center, there is less medium to traverse in the in-plane direction than in the out-of-plane direction (see Fig. 4.8). It is thus expected that the nuclear modification factor depends not only on the transverse momentum, but also on the reaction plane angle: $R_{AA} = R_{AA}(P_T, \phi_{RP})$. The sensitivity of elastic energy loss Monte Carlo model on ϕ_{RP} was studied in Paper [II].

The loss of azimuthal symmetry necessitates the upgrade of the hydrodynamical model. The evolution equations are now (2+1)-dimensional, equation of state is from Ref. [223] and the initial density profile is sWN (entropy density scaling with the number of wounded nucleons, see Chapter 3) with initial time $\tau_0 = 0.17$ fm from the EKRT model. Due to the more advanced EoS, the hydro does not have separate QGP and mixed phases, so the effective temperature (4.2) (without the bag constant) is used at all times in the energy loss simulations. As before, the simulation ends when the system has completely transformed into a hadron gas, which can be considered to happen at $T = 165$ MeV as above.

Overall the simulation setup is very similar to that of central collisions. As an essential new feature, the hard partons within the final rapidity acceptance have been divided in six bins of angle $\Delta\phi$ with respect to the reaction plane, with $\Delta\phi = 0 - 15^\circ$ being closest to in-plane direction and $\Delta\phi = 75 - 90^\circ$ closest to out-of-plane direction. This mimics the reaction plane measurement setup by PHENIX [224]. The strong coupling constant is $\alpha_s = 0.5$, in order to produce enough suppression in the 0-10% centrality bin to match the azimuthally averaged $R_{AA}^{\pi^0}(P_T)$ data. The idea is to examine how well the model, when tuned

to give the right amount of suppression in the central collisions, matches the experimental data in the higher centralities.

Figure 4.9 shows the simulated $R_{AA}^{\pi^0}(P_T, \phi)$ compared with PHENIX data for 0-10%, 40-50% and 50-60% centrality bins. The most obvious disrepancy between the simulation and experimental data occurs in the separation between in-plane and out-of-plane suppression. The experimental data show over a factor two difference between the in-plane R_{AA} and out-of-plane R_{AA} for 40-50% centrality; the elastic energy loss Monte Carlo finds practically no difference between the two directions. Closer examination reveals that the simulation also has too weak a centrality dependence of the suppression: At 40-50% centrality, the angle-averaged $R_{AA}(P_T)$ measured by PHENIX would be between 0.5 and 0.6, while for the simulation it is roughly 0.4. At 50-60% centrality, PHENIX average is roughly 0.65, while in the simulation it is ≈ 0.5.

Apparently the studied elastic energy loss model has too weak a pathlength dependence, as that is what $R_{AA}(P_T, \phi)$ essentially measures. From the static medium case (Fig. 4.2) it is known that the average elastic energy loss depends linearly on distance L traveled in the medium. Radiative energy loss, on the other hand, can achieve L^2 dependence due to the coherence effects, as discussed in Chapter 2. Thus the incoherent nature of elastic scatterings is most likely the reason for the rather dramatic disagreement with the experimental data.

This study is a prime example of the fact that comparing the energy loss model against several experimental observables is an absolute necessity. Within a reasonable range of α_s values, the angular-averaged R_{AA} for any single centrality class could be reproduced by the elastic energy loss model used here (with smaller coupling values towards more peripheral collisions). However, fitting R_{AA} for *all* centrality classes *simultaneously* is not possible; neither can the difference between in-plane and out-of-plane $R_{AA}(P_T, \phi)$ be realized by this model in its current state.

These results also show how the straightforward elastic energy loss modeling serves as a useful baseline, on top of which one must consider more complicated hard-parton+medium-parton interaction mechanisms and coherence effects.

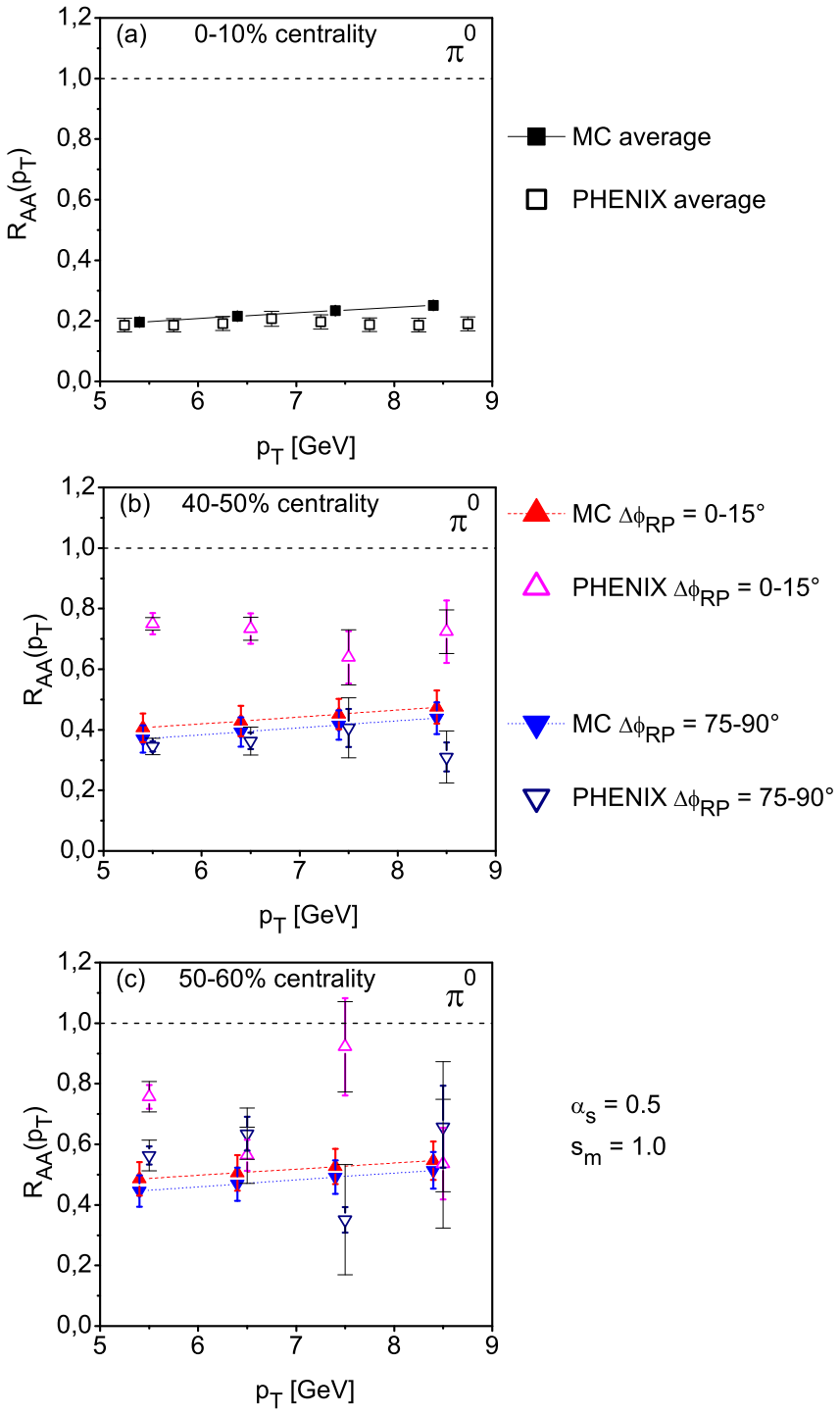

Figure 4.9: The centrality- and reaction plane angle dependence of π^0 nuclear modification factor. The simulation points (solid squares and triangles) are connected with lines for visual guidance. PHENIX data is from [147] (0-10% centrality, open squares) and [224] (40-50% and 50-60% centrality, open triangles). Colored bars with small cap represent statistical errors; black bars with wide cap are systematic errors. From Paper [II].

4.4 From RHIC to LHC

While the reaction plane dependence of R_{AA} at RHIC poses the first challenge for energy loss models, the LHC data introduces two new important sets of constraints. First, the model must be able to produce right amount of suppression at both RHIC and LHC collision energies. Second, the energy loss model must be able to reproduce the increased P_T sensitivity of the nuclear modification factor R_{AA} in the LHC, mentioned already in the beginning of this Chapter.

Figure 4.10 shows how the $R_{AA}(P_T)$ changes in the transition from $\sqrt{s_{NN}} =$ 200 GeV Au+Au collisions at RHIC to $\sqrt{s_{NN}} = 2.76$ TeV Pb+Pb collisions at the LHC [III]. Using the (2+1)-dimensional hydro with a smooth ϵBC profile (defined in Chapter 3) instead of the previously used sWN profile requires the re-tuning of α_s to 0.55 to get the right amount of suppression for neutral pion $R_{AA}(P_T)$ in RHIC. The final rapidity window remains $|y_f| < 0.35$ for RHIC; for the LHC the interval is $|y_f| < 0.8$ to mimic the ALICE result [69], which was used for comparison in Paper [III]. For CMS, $|y_f| < 1.0$; this small difference should not have a significant effect on the results, however.

There are two discrepancies visible between the experimental and Monte Carlo results. First, while the approximate "fit" for RHIC π^0 data is perhaps slightly above the data, at the LHC energies the simulation points are clearly below the data. It thus seems that the MC model has a tendency to overestimate the suppression as the energy density increases. However, because of the difference in the maximum temperatures (≈ 600 MeV at RHIC and ≈ 900 MeV in the LHC), keeping the strong coupling α_s at the same value for both cases might not be correct; a study with the running coupling is needed.

It can also be seen that the model cannot quite reproduce the P_T dependence of R_{AA} measured by CMS. As argued in the static medium study, the rise in $R_{AA}(P_T)$ would be easiest to achieve with a Gaussian-shaped energy loss distribution, where all the particles can be assumed to lose about similar amount of energy. This is not realized in the Monte Carlo model investigated here. Thus a large elastic contribution to the total energy loss is no longer indicated by the LHC data when the diffusion approximation is relieved. This demonstrates the necessity for detailed, rigorous calculations in energy loss modeling.

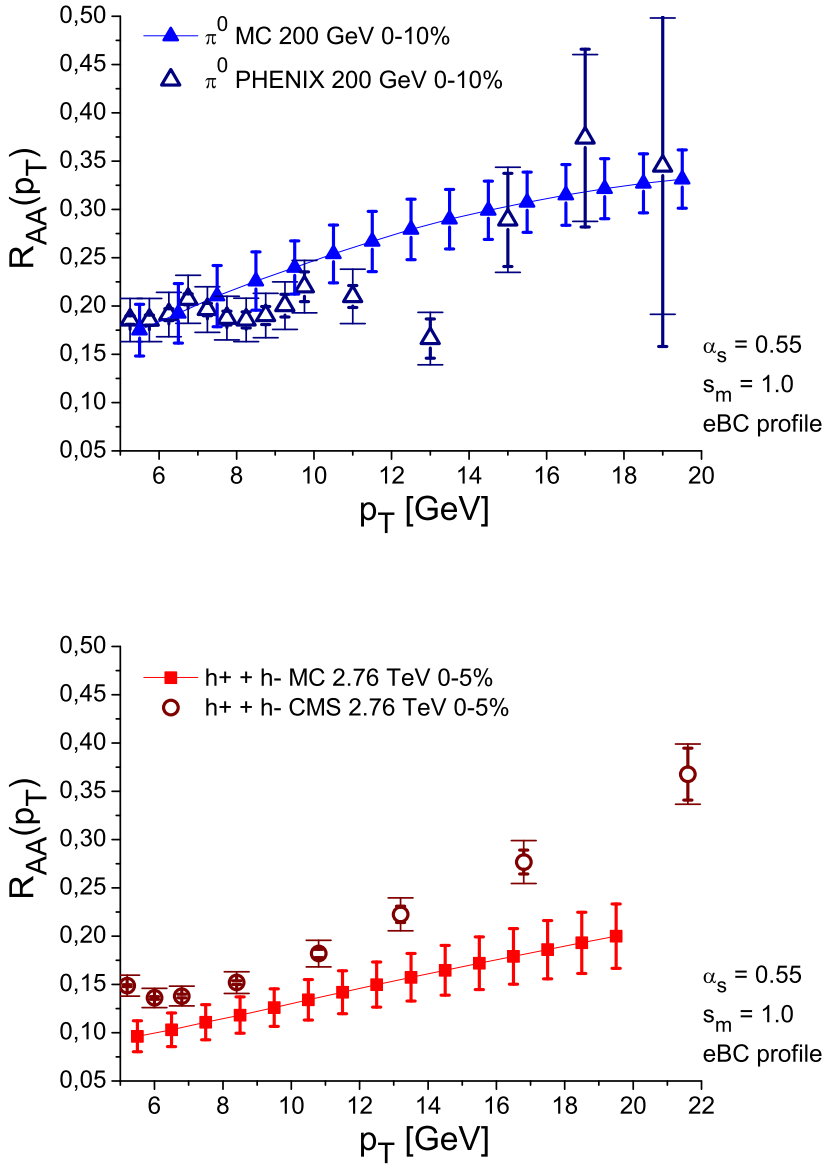

Figure 4.10: Comparison of the elastic energy loss Monte Carlo simulation (MC) and experimental data for neutral pion $R_{AA}(P_T)$ in RHIC $\sqrt{s_{NN}} = 200$ GeV Au+Au collisions and charged hadron $R_{AA}(P_T)$ in LHC $\sqrt{s_{NN}} = 2.76$ TeV Pb+Pb collisions. The simulation points (solid squares and triangles) are connected with lines for visual guidance. The PHENIX data (open triangles) are from [147] and CMS data (open circles) are from [225]. Error bars with small cap represent statistical errors; bars with wide cap are systematic errors.

4.5 Initial state density fluctuations

Except in the unrealistic case of a static medium, the energy loss modeling is always interwoven with the modeling of the hydrodynamical medium. Thus the initial state density fluctuations produced by the modern Monte Carlo Glauber -initiated hydro [199] could potentially have effects on the behavior of the energy loss. With fluctuating initial conditions, the hard partons tend to be formed in "hotspots" where the densities are higher than in the smooth profile; this could potentially increase the parton energy loss. At the same time, there will also be "cold spots" which would have the opposite effect on partons traversing through them. It is not *a priori* clear whether these effects balance out or not.

Also, while in the smooth hydro the densities are always largest in the center (as seen in Fig. 4.7), with fluctuating density profile there might be a hotspot formed close to the edge of the medium, which obviously would effect $R_{AA}(\phi)$: see the Figure 3 in Paper [IV], a pioneering work where the subject of density fluctuations is thoroughly studied.

The hydro setup in this investigation is as in the previous section, the only difference is the lumpiness of the initial density distributions caused by the limited sample of binary collisions in a single heavy ion event (see the description of Monte Carlo Glauber in Chapter 3).

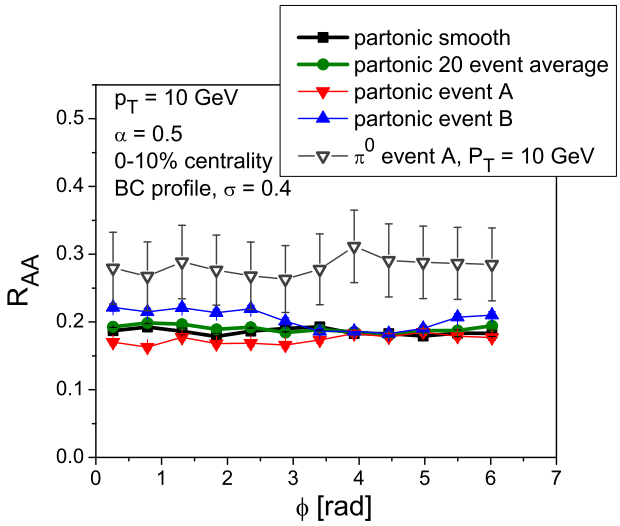

Figure 4.11: The partonic nuclear suppression factor R_{AA} for central $\sqrt{s_{NN}} =$ 200 GeV Au+Au collisions at $p_T = 10$ GeV as a function of the angle of outgoing partons with respect to the event plane shown for smooth initial conditions, for two different events with fluctuating initial conditions and for an average over 20 fluctuation events. Nuclear suppression factor for π^0 at $P_T = 10$ GeV in one event is also displayed. From Paper [IV].

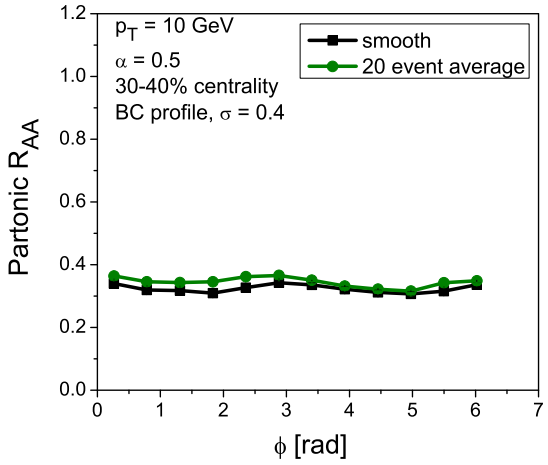

Figure 4.12: The partonic nuclear suppression factor R_{AA} for 30-40% peripheral $\sqrt{s_{NN}} = 200$ GeV Au+Au collisions at $p_T = 10$ GeV, shown as a function of the angle of outgoing partons with respect to the event plane. Solid black squares correspond to the smooth initial conditions, and solid green circles to the average over 20 events with fluctuating initial conditions. From Paper [IV].

Figure 4.11 displays the partonic nuclear suppression factor $R_{AA}(\phi)$ at $p_T = 10$ GeV as a function of the event plane angle ϕ for various different scenarios. There are two single events, A and B; an average over 20 events with fluctuating initial conditions; a smooth hydro result and one single event convoluted with the fragmentation functions to get π^0 nuclear modification. The strong coupling constant has a value $\alpha_s = 0.5$ in all scenarios.

There is a clear variation between single events, so the fluctuating initial densities do have an effect on the nuclear modification as one would expect. However, the experimental results do not originate from one single event but rather are compilations of millions of events. So, to compare with experimental results, an average over several events must be taken. As seen in the Figure, 20 events is already sufficient to show that in central collisions there is very little difference between an event-by-event hydro and a hydro with smooth initial density profiles, when the average over the events is taken.

Figure 4.12 demonstrates the situation in non-central collisions. The average of the events with fluctuating initial conditions is systematically above the smooth initial conditions curve, which would imply that the decreased suppression due to the cold spots is not any more balanced out by the hot spots in higher centralities, and the initial density fluctuations do have an impact on the R_{AA}. However, the difference between the two curves is so small that one is inclined to claim the effect negligible, at least as far as this incoherent energy loss model is concerned.

Chapter 5

Summary and outlook

The energy loss of the high-energy partons in a quark-gluon plasma has intrigued particle physicists since the 1980s, when the hunt for QGP began. The model-building continued throughout the 1990s, but the work intensified in the beginning of the 2000s, when QGP was successfully produced at RHIC and the first data of the suppression of high-energy hadrons was published.

Because of the rich world of physical phenomena involved in (ultra)relativistic heavy ion collisions, modeling the parton energy loss in a strongly interacting medium is a highly nontrivial subfield of QCD. Between different energy loss models, there is considerable variation in the assumptions about the characteristics of the medium and how the hard partons interact with this medium.

In this thesis, a Monte Carlo model for the elastic energy loss of high-energy partons has been developed. All the leading-order 2-to-2 processes have been implemented, and no simplifications have been made on the scattering kinematics or parton propagation trajectories; thermal parton can be soft or hard – as long as the total distribution of the medium particles respects the given thermal distribution – and the scattered partons propagate non-eikonally. Likewise, the scattering itself can be soft or hard, although the overall probability for each type of scattering is limited by the cross section, containing the necessary thermal-mass-like regulator which cuts away the very softest interactions.

An attempt has been made to simulate the collision geometry and the hydrodynamical background with as much detail as possible. The initial starting points of the hard partons are distributed according to the Glauber model. The energy density of the medium varies according to the spacetime position, so do the flow components v_x, v_y and v_z. The hadron gas phase is not taken into account; this is justified by the central collisions study with the bag model hydro, where already the effect of the mixed phase was found to be small (Fig. 4.5). Even the initial state density fluctuations have been implemented, with their hot and cold spots, although this was not found to significantly affect the results (Figs. 4.11 and 4.12).

Beyond the initial density fluctuations, Renk *et al.* [226] have examined the effect of different hydro models on the energy loss and found that the choice of hy-

drodynamical model can effect the results (such as the spread of $R_{AA}(P_T, \phi_{RP})$) by a factor of 2. It remains to be investigated how large the effect is for purely elastic energy loss.

While the angular-averaged $R_{AA}^{\pi^0}(P_T)$ in the most central collisions at RHIC could be successfully reproduced, the pathlength dependence of a model with purely incoherent collisions has been shown here to be in disagreement with the data, as evidenced in Figure 4.9. This shows the importance of testing the model against several observables.

The renaissance of the elastic energy loss models in the 2000s was stimulated mainly by the unexpectedly large suppression of heavy-flavored hadrons. The results for the light quarks presented in this thesis cast doubt also upon the possibility of a large elastic contribution to the heavy quark energy loss.

A rigorous implementation of coherent $2 \to 3$ processes would thus be necessary for a more complete picture of the hard parton energy loss. However, in addition to the more complicated phase space, the coherence effects are challenging to realize properly in a Monte Carlo simulation because of the nonlocality of the problem.

Somewhat simpler potential improvements to the pQCD calculations utilized in the model discussed here would be the renovation of the regularization scheme and the implementation of the running coupling $\alpha_s(Q^2)$, which might help with the transition from RHIC to LHC energy densities (Figure 4.10).

On the other hand, concentrating only on the single-particle observables with leading-particle assumption has left some of the potential of a Monte Carlo simulation untapped, as this kind of framework is ideal for the studies of dihadron correlations and jet broadening (possibly using PYTHIA shower as the baseline). For example, the effect of the surface bias observed in this thesis on the back-to-back jets would warrant an investigation.

With plenty of quality data from RHIC for several different observables (such as $R_{AA}(P_T, \phi_{RP})$ and I_{AA}), and more already coming from the LHC (with more detailed information about jet broadening etc.), the modeling community has a solid experimental foundation to build on. As seen in Chapter 2, the energy loss models have become more and more detailed in the recent years. Thus the need for detailed Monte Carlo modeling is obvious, as the requirement of having a well-tested description of the QCD medium and the necessity of multiobservable analysis are most easily combined in the Monte Carlo simulations.

References

[I] J. Auvinen, K. J. Eskola and T. Renk, Phys. Rev. C **82**, 024906 (2010) [arXiv:0912.2265 [hep-ph]].

[II] J. Auvinen, K. J. Eskola, H. Holopainen and T. Renk, Phys. Rev. C **82**, 051901 (2010) [arXiv:1008.4657 [hep-ph]].

[III] J. Auvinen, K. J. Eskola, H. Holopainen and T. Renk, J. Phys. G **38**, 124160 (2011) [arXiv:1106.4167 [hep-ph]].

[IV] T. Renk, H. Holopainen, J. Auvinen and K. J. Eskola, Phys. Rev. C **85**, 044915 (2012) [arXiv:1105.2647 [hep-ph]].

[V] J. Auvinen and T. Renk, Phys. Rev. C **85**, 037901 (2012) [arXiv:1112.1779 [hep-ph]].

[1] H. Geiger and E. Marsden, Proc. R. Soc. Lond. A **82**, 495 (1909).

[2] E. Rutherford, Phil. Mag. **21**, 669 (1911).

[3] Oxford English Dictionary Online, Oxford University Press. March 2012.

[4] J. Chadwick, Nature **129**, 312 (1932).

[5] L. V. P. R. de Broglie, Annals Phys. **2**, 22 (1925).

[6] E. D. Bloom, D. H. Coward, H. C. DeStaebler, J. Drees, G. Miller, L. W. Mo, R. E. Taylor and M. Breidenbach *et al.*, Phys. Rev. Lett. **23**, 930 (1969).

[7] M. Breidenbach, J. I. Friedman, H. W. Kendall, E. D. Bloom, D. H. Coward, H. C. DeStaebler, J. Drees and L. W. Mo *et al.*, Phys. Rev. Lett. **23**, 935 (1969).

[8] M. Gell-Mann, Phys. Lett. **8**, 214 (1964).

[9] G. Zweig, CERN-TH-412.

[10] W. J. Marciano and H. Pagels, Phys. Rept. **36**, 137 (1978).

[11] J. E. Augustin *et al.* [SLAC-SP-017 Collaboration], Phys. Rev. Lett. **33**, 1406 (1974).

[12] J. J. Aubert *et al.* [E598 Collaboration], Phys. Rev. Lett. **33**, 1404 (1974).

[13] E. G. Cazzoli, A. M. Cnops, P. L. Connolly, R. I. Louttit, M. J. Murtagh, R. B. Palmer, N. P. Samios and T. T. Tso *et al.*, Phys. Rev. Lett. **34**, 1125 (1975).

[14] G. Goldhaber, F. Pierre, G. S. Abrams, M. S. Alam, A. Boyarski, M. Breidenbach, W. C. Carithers and W. Chinowsky *et al.*, Phys. Rev. Lett. **37**, 255 (1976).

[15] I. Peruzzi, M. Piccolo, G. J. Feldman, H. K. Nguyen, J. Wiss, G. S. Abrams, M. S. Alam and A. Boyarski *et al.*, Phys. Rev. Lett. **37**, 569 (1976).

[16] J. C. Collins and M. J. Perry, Phys. Rev. Lett. **34**, 1353 (1975).

[17] N. Cabibbo and G. Parisi, Phys. Lett. B **59**, 67 (1975).

[18] A. M. Polyakov, Phys. Lett. B **72**, 477 (1978).

[19] L. Susskind, Phys. Rev. D **20**, 2610 (1979).

[20] E. V. Shuryak, Phys. Rept. **61**, 71 (1980).

[21] M. Jacob and J. Tran Thanh Van, Phys. Rept. **88**, 325 (1982).

[22] A. Bamberger *et al.* [NA35 Collaboration], Phys. Lett. B **184**, 271 (1987).

[23] U. W. Heinz and M. Jacob, nucl-th/0002042.

[24] http://press.web.cern.ch/press/pressreleases/releases2000/PR01.00EQuarkGluonMatter.html

[25] http://www4.rcf.bnl.gov/brahms/WWW/brahms.html

[26] http://www.phenix.bnl.gov

[27] http://www.phobos.bnl.gov

[28] http://www.star.bnl.gov

[29] I. Arsene *et al.* [BRAHMS Collaboration], Nucl. Phys. A **757**, 1 (2005) [nucl-ex/0410020].

[30] K. Adcox *et al.* [PHENIX Collaboration], Nucl. Phys. A **757**, 184 (2005) [nucl-ex/0410003].

[31] B. B. Back, M. D. Baker, M. Ballintijn, D. S. Barton, B. Becker, R. R. Betts, A. A. Bickley and R. Bindel *et al.*, Nucl. Phys. A **757**, 28 (2005) [nucl-ex/0410022].

[32] J. Adams *et al.* [STAR Collaboration], Nucl. Phys. A **757**, 102 (2005) [nucl-ex/0501009].

[33] http://www.bnl.gov/bnlweb/pubaf/pr/docs/Hunting-the-QGP.pdf

[34] F. Karsch, Nucl. Phys. A **698**, 199 (2002) [hep-ph/0103314].

[35] I. G. Bearden *et al.* [BRAHMS Collaboration], Phys. Rev. Lett. **88**, 202301 (2002) [nucl-ex/0112001].

[36] S. S. Adler *et al.* [PHENIX Collaboration], Phys. Rev. C **71**, 034908 (2005) [Erratum-ibid. C **71**, 049901 (2005)] [nucl-ex/0409015].

[37] B. B. Back, M. D. Baker, D. S. Barton, R. R. Betts, M. Ballintijn, A. A. Bickley, R. Bindel and A. Budzanowski *et al.*, Phys. Rev. Lett. **91**, 052303 (2003) [nucl-ex/0210015].

[38] J. Adams *et al.* [STAR Collaboration], Phys. Rev. C **70**, 054907 (2004) [nucl-ex/0407003].

[39] K. Adcox *et al.* [PHENIX Collaboration], Phys. Rev. Lett. **89**, 212301 (2002) [nucl-ex/0204005].

[40] J. Adams *et al.* [STAR Collaboration], Phys. Rev. C **72**, 014904 (2005) [nucl-ex/0409033].

[41] A. Adare *et al.* [PHENIX Collaboration], Phys. Rev. Lett. **98**, 162301 (2007) [nucl-ex/0608033].

[42] S. S. Adler *et al.* [PHENIX Collaboration], Phys. Rev. Lett. **91**, 072301 (2003) [nucl-ex/0304022].

[43] S. S. Adler *et al.* [PHENIX Collaboration], Phys. Rev. C **69**, 034910 (2004) [nucl-ex/0308006].

[44] J. Adams *et al.* [STAR Collaboration], Phys. Rev. Lett. **91**, 172302 (2003) [nucl-ex/0305015].

[45] S. S. Adler *et al.* [PHENIX Collaboration], Phys. Rev. Lett. **91**, 072303 (2003) [nucl-ex/0306021].

[46] J. Adams *et al.* [STAR Collaboration], Phys. Rev. Lett. **91**, 072304 (2003) [nucl-ex/0306024].

[47] D. Kharzeev, E. Levin and L. McLerran, Phys. Lett. B **561**, 93 (2003) [hep-ph/0210332].

[48] S. S. Adler *et al.* [PHENIX Collaboration], Phys. Rev. Lett. **94**, 232301 (2005) [nucl-ex/0503003].

[49] C. Adler *et al.* [STAR Collaboration], Phys. Rev. Lett. **90**, 082302 (2003) [nucl-ex/0210033].

[50] A. Adare *et al.* [PHENIX Collaboration], Phys. Rev. C **78**, 014901 (2008) [arXiv:0801.4545 [nucl-ex]].

[51] T. Renk and K. J. Eskola, Phys. Rev. C **84**, 054913 (2011) [arXiv:1106.1740 [hep-ph]].

[52] http://aliceinfo.cern.ch/Public/

[53] http://atlas.ch/

[54] http://cern.ch/cms

[55] http://lhcb-public.web.cern.ch/lhcb-public/

[56] http://cern.ch/totem-experiment/

[57] O. Adriani *et al.* [LHCf Collaboration], JINST **3**, S08006 (2008).

[58] http://moedal.web.cern.ch/

[59] B. Abelev *et al.* [ALICE Collaboration], Phys. Rev. Lett. **105**, 252301 (2010) [arXiv:1011.3916 [nucl-ex]].

[60] G. Aad *et al.* [ATLAS Collaboration], Phys. Lett. B **710**, 363 (2012) [arXiv:1108.6027 [hep-ex]].

[61] S. Chatrchyan *et al.* [CMS Collaboration], JHEP **1108**, 141 (2011) [arXiv:1107.4800 [nucl-ex]].

[62] KAamodt *et al.* [The ALICE Collaboration], Phys. Rev. Lett. **105**, 252302 (2010) [arXiv:1011.3914 [nucl-ex]].

[63] G. Aad *et al.* [ATLAS Collaboration], Phys. Lett. B **707**, 330 (2012) [arXiv:1108.6018 [hep-ex]].

[64] V. Zhukova [CMS Collaboration], J. Phys. G G **38**, 124046 (2011).

[65] A. Trzupek [ATLAS Collaboration], J. Phys. G G **38**, 124163 (2011).

[66] K. Aamodt *et al.* [ALICE Collaboration], Phys. Rev. Lett. **107**, 032301 (2011) [arXiv:1105.3865 [nucl-ex]].

[67] J. Velkovska [CMS Collaboration], J. Phys. G G **38**, 124011 (2011).

[68] B. Schenke, S. Jeon and C. Gale, Phys. Lett. B **702**, 59 (2011) [arXiv:1102.0575 [hep-ph]].

[69] K. Aamodt *et al.* [ALICE Collaboration], Phys. Lett. B **696**, 30 (2011) [arXiv:1012.1004 [nucl-ex]].

[70] H. Appelshauser, J. Phys. G G **38**, 124014 (2011) [arXiv:1110.0638 [nucl-ex]].

[71] Y. -J. Lee [for the CMS Collaboration], J. Phys. G G **38**, 124015 (2011) [arXiv:1107.2131 [hep-ex]].

[72] A. Milov, J. Phys. G G **38**, 124113 (2011) [arXiv:1107.0460 [nucl-ex]].

[73] J. F. Grosse-Oetringhaus, J. Phys. G G **38**, 124028 (2011) [arXiv:1107.0556 [nucl-ex]].

[74] T. Renk and K. J. Eskola, Phys. Rev. C **77**, 044905 (2008) [arXiv:0711.3303 [hep-ph]].

[75] G. Aad *et al.* [ATLAS Collaboration], Phys. Rev. Lett. **105**, 252303 (2010) [arXiv:1011.6182 [hep-ex]].

[76] S. Chatrchyan *et al.* [CMS Collaboration], Phys. Rev. C **84**, 024906 (2011) [arXiv:1102.1957 [nucl-ex]].

[77] M. Luo, J. -w. Qiu and G. F. Sterman, Phys. Lett. B **279**, 377 (1992).

[78] M. Luo, J. -w. Qiu and G. F. Sterman, Phys. Rev. D **49**, 4493 (1994).

[79] M. Luo, J. -w. Qiu and G. F. Sterman, Phys. Rev. D **50**, 1951 (1994).

[80] X. -f. Guo and X. -N. Wang, Phys. Rev. Lett. **85**, 3591 (2000) [hep-ph/0005044].

[81] X. -N. Wang and X. -f. Guo, Nucl. Phys. A **696**, 788 (2001) [hep-ph/0102230].

[82] A. Majumder and B. Muller, Phys. Rev. C **77**, 054903 (2008) [arXiv:0705.1147 [nucl-th]].

[83] A. Majumder, R. J. Fries and B. Muller, Phys. Rev. C **77**, 065209 (2008) [arXiv:0711.2475 [nucl-th]].

[84] A. Majumder, arXiv:0901.4516 [nucl-th].

[85] A. Majumder, Phys. Rev. D **85**, 014023 (2012) [arXiv:0912.2987 [nucl-th]].

[86] I. P. Lokhtin and A. M. Snigirev, Eur. Phys. J. C **45**, 211 (2006) [hep-ph/0506189].

[87] I. P. Lokhtin, L. V. Malinina, S. V. Petrushanko, A. M. Snigirev, I. Arsene and K. Tywoniuk, PoS HIGH **-PTLHC08**, 002 (2008) [arXiv:0810.2082 [hep-ph]].

[88] N. Armesto, L. Cunqueiro and C. A. Salgado, Eur. Phys. J. C **63**, 679 (2009) [arXiv:0907.1014 [hep-ph]].

[89] K. Zapp, G. Ingelman, J. Rathsman, J. Stachel and U. A. Wiedemann, Eur. Phys. J. C **60**, 617 (2009) [arXiv:0804.3568 [hep-ph]].

[90] K. C. Zapp, F. Krauss and U. A. Wiedemann, arXiv:1111.6838 [hep-ph].

[91] T. Renk, Phys. Rev. C **78**, 034908 (2008) [arXiv:0806.0305 [hep-ph]].

[92] T. Renk, Phys. Rev. C **79**, 054906 (2009) [arXiv:0901.2818 [hep-ph]].

[93] T. Renk, Phys. Rev. C **81**, 014906 (2010) [arXiv:0910.3528 [hep-ph]].

[94] T. Renk, Phys. Rev. C **83**, 024908 (2011) [arXiv:1010.4116 [hep-ph]].

[95] J. D. Bjorken, FERMILAB-PUB-82-059-THY.

[96] F. Niedermayer, Phys. Rev. D **34**, 3494 (1986).

[97] M. Gyulassy and M. Plumer, Nucl. Phys. A **527**, 641 (1991).

[98] B. Svetitsky, Phys. Rev. D **37**, 2484 (1988).

[99] M. H. Thoma and M. Gyulassy, Nucl. Phys. B **351**, 491 (1991).

[100] M. Le Bellac, Cambridge, UK: Univ. Pr. (1996) 270 p

[101] E. Braaten and M. H. Thoma, Phys. Rev. D **44**, 1298 (1991).

[102] E. Braaten and M. H. Thoma, Phys. Rev. D **44**, 2625 (1991).

[103] J. F. Gunion and G. Bertsch, Phys. Rev. D **25**, 746 (1982).

[104] M. Gyulassy, M. Plumer, M. Thoma and X. N. Wang, Nucl. Phys. A **538**, 37C (1992).

[105] M. H. Thoma and M. Gyulassy, Nucl. Phys. A **544**, 573C (1992).

[106] M. Gyulassy and X. -N. Wang, Nucl. Phys. B **420**, 583 (1994) [nucl-th/9306003].

[107] X. -N. Wang, M. Gyulassy and M. Plumer, Phys. Rev. D **51**, 3436 (1995) [hep-ph/9408344].

[108] A. B. Migdal, Phys. Rev. **103**, 1811 (1956).

[109] R. Baier, Y. L. Dokshitzer, S. Peigne and D. Schiff, Phys. Lett. B **345**, 277 (1995) [hep-ph/9411409].

[110] R. Baier, Y. L. Dokshitzer, A. H. Mueller, S. Peigne and D. Schiff, Nucl. Phys. B **478**, 577 (1996) [hep-ph/9604327].

[111] R. Baier, Y. L. Dokshitzer, A. H. Mueller, S. Peigne and D. Schiff, Nucl. Phys. B **483**, 291 (1997) [hep-ph/9607355].

[112] R. Baier, Y. L. Dokshitzer, A. H. Mueller, S. Peigne and D. Schiff, Nucl. Phys. B **484**, 265 (1997) [hep-ph/9608322].

[113] R. Baier, Y. L. Dokshitzer, A. H. Mueller and D. Schiff, Phys. Rev. C **58**, 1706 (1998) [hep-ph/9803473].

[114] J. D. Bjorken, Phys. Rev. D **27**, 140 (1983).

[115] B. G. Zakharov [Landau Institute for Theoretical Physics, Moscow Collaboration], JETP Lett. **63**, 952 (1996) [hep-ph/9607440].

[116] B. G. Zakharov [LPTHE, Univ. de Paris-Sud, Orsay and L. D. Landau Institute for Theoretical Physics, Moscow, Russia Collaboration], JETP Lett. **65**, 615 (1997) [hep-ph/9704255].

[117] B. G. Zakharov, Phys. Atom. Nucl. **61**, 838 (1998) [Yad. Fiz. **61**, 924 (1998)] [hep-ph/9807540].

[118] R. Baier, Y. L. Dokshitzer, A. H. Mueller and D. Schiff, Nucl. Phys. B **531**, 403 (1998) [hep-ph/9804212].

[119] M. Gyulassy, P. Levai and I. Vitev, Nucl. Phys. B **571**, 197 (2000) [hep-ph/9907461].

[120] M. Gyulassy, P. Levai and I. Vitev, Nucl. Phys. A **661**, 637 (1999) [hep-ph/9907343].

[121] M. Gyulassy, P. Levai and I. Vitev, Nucl. Phys. B **594**, 371 (2001) [nucl-th/0006010].

[122] M. Gyulassy, P. Levai and I. Vitev, Phys. Rev. Lett. **85**, 5535 (2000) [nucl-th/0005032].

[123] M. Gyulassy, P. Levai and I. Vitev, Phys. Lett. B **538**, 282 (2002) [nucl-th/0112071].

[124] M. Gyulassy, I. Vitev and X. N. Wang, Phys. Rev. Lett. **86**, 2537 (2001) [nucl-th/0012092].

[125] M. Gyulassy, I. Vitev, X. -N. Wang and P. Huovinen, Phys. Lett. B **526**, 301 (2002) [nucl-th/0109063].

[126] M. Djordjevic and M. Gyulassy, Nucl. Phys. A **733**, 265 (2004) [nucl-th/0310076].

[127] Y. L. Dokshitzer and D. E. Kharzeev, Phys. Lett. B **519**, 199 (2001) [hep-ph/0106202].

[128] U. A. Wiedemann and M. Gyulassy, Nucl. Phys. B **560**, 345 (1999) [hep-ph/9906257].

[129] U. A. Wiedemann, Nucl. Phys. B **582**, 409 (2000) [hep-ph/0003021].

[130] U. A. Wiedemann, Nucl. Phys. B **588**, 303 (2000) [hep-ph/0005129].

[131] W. H. Furry, Phys. Rev. **46**, 391 (1934).

[132] C. A. Salgado and U. A. Wiedemann, Phys. Rev. D **68**, 014008 (2003) [hep-ph/0302184].

[133] R. Baier, Y. L. Dokshitzer, A. H. Mueller and D. Schiff, JHEP **0109**, 033 (2001) [hep-ph/0106347].

[134] K. J. Eskola, H. Honkanen, C. A. Salgado and U. A. Wiedemann, Nucl. Phys. A **747**, 511 (2005) [hep-ph/0406319].

[135] N. Armesto, C. A. Salgado and U. A. Wiedemann, Phys. Rev. D **69**, 114003 (2004) [hep-ph/0312106].

[136] P. B. Arnold, G. D. Moore and L. G. Yaffe, JHEP **0111**, 057 (2001) [hep-ph/0109064].

[137] P. B. Arnold, G. D. Moore and L. G. Yaffe, JHEP **0112**, 009 (2001) [hep-ph/0111107].

[138] P. B. Arnold, G. D. Moore and L. G. Yaffe, JHEP **0206**, 030 (2002) [hep-ph/0204343].

[139] P. B. Arnold, G. D. Moore and L. G. Yaffe, JHEP **0301**, 030 (2003) [hep-ph/0209353].

[140] S. Turbide, C. Gale, S. Jeon and G. D. Moore, Phys. Rev. C **72**, 014906 (2005) [hep-ph/0502248].

[141] G. -Y. Qin, J. Ruppert, C. Gale, S. Jeon, G. D. Moore and M. G. Mustafa, Phys. Rev. Lett. **100**, 072301 (2008) [arXiv:0710.0605 [hep-ph]].

[142] B. Schenke, C. Gale and G. -Y. Qin, Phys. Rev. C **79**, 054908 (2009) [arXiv:0901.3498 [hep-ph]].

[143] Y. L. Dokshitzer, Sov. Phys. JETP **46**, 641 (1977) [Zh. Eksp. Teor. Fiz. **73**, 1216 (1977)].

[144] V. N. Gribov and L. N. Lipatov, Sov. J. Nucl. Phys. **15**, 438 (1972) [Yad. Fiz. **15**, 781 (1972)].

[145] G. Altarelli and G. Parisi, Nucl. Phys. B **126**, 298 (1977).

[146] E. Wang and X. -N. Wang, Phys. Rev. Lett. **89**, 162301 (2002) [hep-ph/0202105].

[147] A. Adare *et al.* [PHENIX Collaboration], Phys. Rev. Lett. **101**, 232301 (2008) [arXiv:0801.4020 [nucl-ex]].

[148] X. -F. Chen, C. Greiner, E. Wang, X. -N. Wang and Z. Xu, Phys. Rev. C **81**, 064908 (2010) [arXiv:1002.1165 [nucl-th]].

[149] X. -F. Chen, T. Hirano, E. Wang, X. -N. Wang and H. Zhang, Phys. Rev. C **84**, 034902 (2011) [arXiv:1102.5614 [nucl-th]].

[150] A. Majumder and C. Shen, arXiv:1103.0809 [hep-ph].

[151] J. Bielcik [STAR Collaboration], Nucl. Phys. A **774**, 697 (2006) [nucl-ex/0511005].

[152] A. Adare *et al.* [PHENIX Collaboration], Phys. Rev. Lett. **98**, 172301 (2007) [nucl-ex/0611018].

[153] M. G. Mustafa and M. H. Thoma, Acta Phys. Hung. A **22**, 93 (2005) [hep-ph/0311168].

[154] M. H. Thoma, Phys. Lett. B **273**, 128 (1991).

[155] M. G. Mustafa, Phys. Rev. C **72**, 014905 (2005) [hep-ph/0412402].

[156] A. K. Dutt-Mazumder, J. -eAlam, P. Roy and B. Sinha, Phys. Rev. D **71**, 094016 (2005) [hep-ph/0411015].

[157] S. Wicks, W. Horowitz, M. Djordjevic and M. Gyulassy, Nucl. Phys. A **784**, 426 (2007) [nucl-th/0512076].

[158] W. A. Horowitz and M. Gyulassy, Nucl. Phys. A **872**, 265 (2011) [arXiv:1104.4958 [hep-ph]].

[159] M. Djordjevic, Phys. Rev. C **74**, 064907 (2006) [nucl-th/0603066].

[160] X. -N. Wang, Phys. Lett. B **650**, 213 (2007) [nucl-th/0604040].

[161] A. Majumder, Phys. Rev. C **80**, 031902 (2009) [arXiv:0810.4967 [nucl-th]].

[162] P. B. Gossiaux and J. Aichelin, Phys. Rev. C **78**, 014904 (2008) [arXiv:0802.2525 [hep-ph]].

[163] P. B. Gossiaux, R. Bierkandt and J. Aichelin, Phys. Rev. C **79**, 044906 (2009) [arXiv:0901.0946 [hep-ph]].

[164] P. B. Gossiaux and J. Aichelin, J. Phys. G G **36**, 064028 (2009) [arXiv:0901.2462 [nucl-th]].

[165] Y. L. Dokshitzer, G. Marchesini and B. R. Webber, Nucl. Phys. B **469**, 93 (1996) [hep-ph/9512336].

[166] P. F. Kolb and U. W. Heinz, In *Hwa, R.C. (ed.) et al.: Quark gluon plasma* 634-714 [nucl-th/0305084].

[167] T. Sjostrand, S. Mrenna and P. Z. Skands, JHEP **0605**, 026 (2006) [hep-ph/0603175].

[168] T. Sjostrand, S. Mrenna and P. Z. Skands, Comput. Phys. Commun. **178**, 852 (2008) [arXiv:0710.3820 [hep-ph]].

[169] B. Andersson, G. Gustafson, G. Ingelman and T. Sjostrand, Phys. Rept. **97**, 31 (1983).

[170] X. -N. Wang and M. Gyulassy, Phys. Rev. D **44**, 3501 (1991).

[171] R. Baier, Y. L. Dokshitzer, A. H. Mueller and D. Schiff, Phys. Rev. C **60**, 064902 (1999) [hep-ph/9907267].

[172] R. Baier, Y. L. Dokshitzer, A. H. Mueller and D. Schiff, Phys. Rev. C **64**, 057902 (2001) [hep-ph/0105062].

[173] U. Abeysekara *et al.* [ALICE EMCal Collaboration], arXiv:1008.0413 [physics.ins-det].

[174] K. Zapp, J. Stachel and U. A. Wiedemann, Phys. Rev. Lett. **103**, 152302 (2009) [arXiv:0812.3888 [hep-ph]].

[175] K. C. Zapp, J. Stachel and U. A. Wiedemann, JHEP **1107**, 118 (2011) [arXiv:1103.6252 [hep-ph]].

[176] R. Baier, A. H. Mueller and D. Schiff, Phys. Lett. B **649**, 147 (2007) [nucl-th/0612068].

[177] H. Liu, K. Rajagopal and U. A. Wiedemann, JHEP **0703**, 066 (2007) [hep-ph/0612168].

[178] T. Renk, Phys. Rev. C **84**, 067902 (2011) [arXiv:1110.2313 [hep-ph]].

[179] C. Nonaka and S. A. Bass, Phys. Rev. C **75**, 014902 (2007) [nucl-th/0607018].

[180] T. Renk, H. Holopainen, R. Paatelainen and K. J. Eskola, Phys. Rev. C **84**, 014906 (2011) [arXiv:1103.5308 [hep-ph]].

[181] B. Schenke, C. Gale and S. Jeon, Phys. Rev. C **80**, 054913 (2009) [arXiv:0909.2037 [hep-ph]].

[182] G. -Y. Qin, J. Ruppert, S. Turbide, C. Gale, C. Nonaka and S. A. Bass, Phys. Rev. C **76**, 064907 (2007) [arXiv:0705.2575 [hep-ph]].

[183] P. F. Kolb, J. Sollfrank and U. W. Heinz, Phys. Rev. C **62**, 054909 (2000) [hep-ph/0006129].

[184] P. F. Kolb and R. Rapp, Phys. Rev. C **67**, 044903 (2003) [hep-ph/0210222].

[185] B. Schenke, S. Jeon and C. Gale, Phys. Rev. C **82**, 014903 (2010) [arXiv:1004.1408 [hep-ph]].

[186] C. Young, B. Schenke, S. Jeon and C. Gale, Phys. Rev. C **84**, 024907 (2011) [arXiv:1103.5769 [nucl-th]].

[187] Z. Xu and C. Greiner, Phys. Rev. C **71**, 064901 (2005) [hep-ph/0406278].

[188] Z. Xu and C. Greiner, Phys. Rev. C **76**, 024911 (2007) [hep-ph/0703233].

[189] O. Fochler, Z. Xu and C. Greiner, Phys. Rev. C **82**, 024907 (2010) [arXiv:1003.4380 [hep-ph]].

[190] J. Uphoff, O. Fochler, Z. Xu and C. Greiner, Phys. Rev. C **84**, 024908 (2011) [arXiv:1104.2295 [hep-ph]].

[191] B. Zhang, Comput. Phys. Commun. **109**, 193 (1998) [nucl-th/9709009].

[192] D. Molnar and M. Gyulassy, Phys. Rev. C **62**, 054907 (2000) [nucl-th/0005051].

[193] V. Borchers, J. Meyer, S. Gieseke, G. Martens and C. C. Noack, Phys. Rev. C **62**, 064903 (2000) [hep-ph/0006038].

[194] S. A. Bass, B. Muller and D. K. Srivastava, Phys. Lett. B **551**, 277 (2003) [nucl-th/0207042].

[195] Z. Xu and C. Greiner, Phys. Rev. C **79**, 014904 (2009) [arXiv:0811.2940 [hep-ph]].

[196] O. Fochler, J. Uphoff, Z. Xu and C. Greiner, J. Phys. G G **38**, 124152 (2011) [arXiv:1107.0130 [hep-ph]].

[197] R. D. Woods and D. S. Saxon, Phys. Rev. **95**, 577 (1954).

[198] M. L. Miller, K. Reygers, S. J. Sanders and P. Steinberg, Ann. Rev. Nucl. Part. Sci. **57**, 205 (2007) [nucl-ex/0701025].

[199] H. Holopainen, H. Niemi and K. J. Eskola, Phys. Rev. C **83**, 034901 (2011) [arXiv:1007.0368 [hep-ph]].

[200] A. Chodos, R. L. Jaffe, K. Johnson, C. B. Thorn and V. F. Weisskopf, Phys. Rev. D **9**, 3471 (1974).

[201] P. Huovinen and P. Petreczky, Nucl. Phys. A **837**, 26 (2010) [arXiv:0912.2541 [hep-ph]].

[202] P. F. Kolb, U. W. Heinz, P. Huovinen, K. J. Eskola and K. Tuominen, Nucl. Phys. A **696**, 197 (2001) [hep-ph/0103234].

[203] K. J. Eskola, K. Kajantie, P. V. Ruuskanen and K. Tuominen, Nucl. Phys. B **570**, 379 (2000) [hep-ph/9909456].

[204] K. J. Eskola, K. Kajantie and J. Lindfors, Nucl. Phys. B **323**, 37 (1989).

[205] K. J. Eskola, H. Honkanen, H. Niemi, P. V. Ruuskanen and S. S. Räsänen, Phys. Rev. C **72**, 044904 (2005) [hep-ph/0506049].

[206] F. Cooper and G. Frye, Phys. Rev. D **10**, 186 (1974).

[207] J. C. Collins, D. E. Soper and G. F. Sterman, Adv. Ser. Direct. High Energy Phys. **5**, 1 (1988) [arXiv:hep-ph/0409313].

[208] K. J. Eskola and H. Honkanen, Nucl. Phys. A **713**, 167 (2003) [arXiv:hep-ph/0205048].

[209] B. L. Combridge, J. Kripfganz and J. Ranft, Phys. Lett. B **70**, 234 (1977).

[210] J. Pumplin, D. R. Stump, J. Huston, H. L. Lai, P. M. Nadolsky and W. K. Tung, JHEP **0207**, 012 (2002) [hep-ph/0201195].

[211] D. Stump, J. Huston, J. Pumplin, W. -K. Tung, H. L. Lai, S. Kuhlmann and J. F. Owens, JHEP **0310**, 046 (2003) [hep-ph/0303013].

[212] M. Arneodo, Phys. Rept. **240**, 301 (1994).

[213] K. J. Eskola, V. J. Kolhinen and P. V. Ruuskanen, Nucl. Phys. B **535**, 351 (1998) [hep-ph/9802350].

[214] K. J. Eskola, V. J. Kolhinen and C. A. Salgado, Eur. Phys. J. C **9**, 61 (1999) [hep-ph/9807297].

[215] M. Hirai, S. Kumano and T. -H. Nagai, Phys. Rev. C **76**, 065207 (2007) [arXiv:0709.3038 [hep-ph]].

[216] K. J. Eskola, H. Paukkunen and C. A. Salgado, JHEP **0904**, 065 (2009) [arXiv:0902.4154 [hep-ph]].

[217] D. de Florian, R. Sassot, P. Zurita and M. Stratmann, Phys. Rev. D **85**, 074028 (2012) [arXiv:1112.6324 [hep-ph]].

[218] T. Matsui, B. Svetitsky and L. D. McLerran, Phys. Rev. D **34**, 783 (1986) [Erratum-ibid. D **37**, 844 (1988)].

[219] B. A. Kniehl, G. Kramer and B. Potter, Nucl. Phys. B **582**, 514 (2000) [hep-ph/0010289].

[220] N. Armesto, B. Cole, C. Gale, W. A. Horowitz, P. Jacobs, S. Jeon, M. van Leeuwen and A. Majumder *et al.*, arXiv:1106.1106 [hep-ph].

[221] T. Renk, K. J. Eskola, PoS **LHC07**, 032 (2007).

[222] T. Renk, arXiv:1112.2503 [hep-ph].

[223] M. Laine and Y. Schroder, Phys. Rev. D **73**, 085009 (2006) [hep-ph/0603048].

[224] S. Afanasiev *et al.* [PHENIX Collaboration], Phys. Rev. C **80**, 054907 (2009) [arXiv:0903.4886 [nucl-ex]].

[225] S. Chatrchyan *et al.* [CMS Collaboration], Eur. Phys. J. C **72**, 1945 (2012) [arXiv:1202.2554 [nucl-ex]].

[226] T. Renk, H. Holopainen, U. Heinz and C. Shen, Phys. Rev. C **83**, 014910 (2011) [arXiv:1010.1635 [hep-ph]].